의학박사 학위논문

Plasticity of input-output relationship mediated by Group I metabotropic glutamate receptors in CA1 pyramidal neurons

CA1 피라미드 세포의 입출력 관계 가소성에 대한 1 군 대사성 글루탐산 수용체의 작용 기전 연구

2019 년 2 월

서울대학교 대학원

의과학과 생리학 전공

김 혜 현

A thesis of the Degree of Doctor of Philosophy

CA1 피라미드 세포의 입출력 관계 가소성에 대한 1군 대사성 글루탐산 수용체의 작용 기전 연구

Plasticity of input-output relationship mediated by Group I metabotropic glutamate receptors in CA1 pyramidal neurons

February 2019

The Department of Biomedical Sciences

Seoul National University

College of Medicine

Hye Hyun Kim

ABSTRACT

Glutamate is a major neurotransmitter in the brain that activates ionotropic and metabotropic glutamate receptors (iGluRs and mGluRs, respectively). The two types of glutamate receptors interact with each other, as exemplified by the modulation of iGluRs by mGluRs. However, the other way of interaction (i.e, modulation of mGluRs by iGluRs) has not received much attention. In this study, I found that group I mGluR-specific agonist, (RS)-3,5-dihydroxyphenylglycine (DHPG), alone is not sufficient to activate phospholipase C (PLC) in rat hippocampus, while glutamate that activates both iGluRs and mGluRs robustly activates PLC. These results suggested that additional mechanisms provided by iGluRs are involved in group I mGluR-mediated PLC activation. I found that AMPA receptors initiate Ca^{2+} influx through L-type Ca^{2+} channels that is specifically required for mGluR-mediated PLC activation. Furthermore, this mechanism is crucial for mGluR-LTD in the hippocampus induced by paired-pulse low frequency synaptic stimulation (PP-LFS). Although PP-LFS induced synaptic depression, it paradoxical increased input-output relationship. I provided evidence that after PP-LFS, robust expression of LTD at inhibitory synapses

(i-LTD) is induced via mGluR-dependent endocannabinoid (eCB) signaling pathway, which leads to reduction of tonic GABA currents that accompanied with significant hyperpolarization of AP threshold (V_{th}) that results in EPSP to spike (E-S) potentiation and increased AP output. By contrast, DHPG induced LTD at excitatory synapses, but hardly induced i-LTD. These results indicated that disinhibition of GABAergic input via mGluR-dependent eCB signaling is responsible for the increase in input-output relationship in spite of synaptic depression during LTD and it is specific to conditioning protocol, PP-LFS.

Keywords: CA1 pyramidal neuron, mGluR5, PLC, Ca^{2+}, electrophysiology, mGluR-LTD, eCB, tonic inhibition, input-output relationship

Student Number: 2011-23798

CONTENTS

LIST OF FIGURES

LIST OF ABBREVIATIONS

antGABARs	GABA receptors antagonist
CaTs	Ca^{2+} transients
$[Ca^{2+}]_i$	intracellular (Cytosolic) Ca^{2+} concentration
Ctrl	control
$\Delta F/F_0$	PHδ-GFP translocation
dpt	Days post-transfection
DHPG	(RS)-3,5-dihydroxyphenylglycine
eCB	Endocannabinoid
ER	Endoplasmic reticulum
E-S	EPSP to spike
I_{GABAR}	GABARs-mediated current
iGluR	ionotripic glutamate receptor
LTCC	L-type Ca^{2+} channel
LTD	Long term depression
LTP	Long term potentiation
mGluR	metabotropic glutamate receptor
NT control	Non-targeted control

PHδ-GFP	Green fluorescent protein (GFP)-labeled PLCδ-pleckstrin homology domain
PKC	Phosphokinase C
PLC	Phospholipase C
PP-LFS	Paired pulse low frequency synaptic stimulation
R_i	Input resistance
RMP	Resting membrane potential
RyR	Ryanodine receptor
SC	Schaffer collateral
shRNA	Short-hairpin RNA
VGCC	Voltage-gated Ca^{2+} channel
V_{th}_ramp	Somatic ramp current injection induced AP threshold
V_{th}_SC	SC fiber stimulation induced AP threshold
V_{th}_PP	perforant pathway stimulation induced AP threshold

INTRODUCTION

1. Group I mGluRs and signaling mechanisms

The metabotropic glutamate receptors (mGluRs) are members of the G protein-coupled receptors that participate in the modulation of synaptic transmission and neuronal excitability throughout the central nervous system (CNS). The existence of mGluRs provides a mechanism by which glutamate, that serves as the neurotransmitter at the majority of excitatory synapses in the CNS, can modulate cell excitability and synaptic transmission via second messenger signaling pathways. Another impotant glutamate receptor activated by glutamate is ionotropic glutamate receptors (iGluRs) that are ligand-gated ion channels which mediate fast excitatory postsynaptic currents. Regulation of iGluRs by mGluRs is previously suggested to be important for integrative brain function (Doherty et al., 1997; Mannaioni et al., 2001). Surface expression of AMPA receptors are reduced by group I mGluR signaling to induce long-term depression (LTD) of synaptic currents (Luscher and Huber, 2010), while NMDA currents are potentiated by group I

mGluR agonists (Doherty et al., 1997). Importantly, impaired function of NMDA receptors in pathologic conditions could be reversed by the up-regulation of group I mGluRs (Won et al., 2012), suggesting a possibility that this interaction can be applied to develop new therapeutic strategies. Likewise, the regulation of mGluRs signaling by iGluRs may also have certain physiological significance, but this possibility has received relatively little attention.

While group I mGluRs (mGluR1 and mGluR5) link glutamatergic neurotransmission to a wide variety of signaling pathways and involve multiple partners (Conn and Pin, 1997), the Gq protein/phospholipase C (PLC)/inositol-3,4,5-triphosphate (IP_3) signal cascades have been considered as the canonical pathway (Abe et al., 1992; Aramori and Nakanishi, 1992). However, the involvement of PLC in group I mGluR effects is not consistent between independent studies. The stimulation of schaffer collateral (SC)-CA1 neuron synapse activates group I mGluRs to mobilize intracellular Ca^{2+} by PLC and IP_3 signal pathways (El-Hassar et al., 2011; Nakamura et al.,

1999; Nakamura et al., 2000), but Ca^{2+} release by the group I mGluR agonist, (RS)-3,5-dihydroxyphenylglycine (DHPG), were shown to be PLC-independent (Sohn et al., 2011). In addition, mGluR-dependent LTD induced by DHPG occurs independently of PLC/IP_3-dependent Ca^{2+} release or protein kinase C (PKC) activity at the SC-CA1 neuron synapse (Fitzjohn et al., 2001; Mockett et al., 2011; Schnabel et al., 1999), whereas mGluR-dependent LTD at the same synapse induced by synaptic stimulation is dependent on intracellular Ca^{2+} rise and PKC activation (Bolshakov and Siegelbaum, 1994; Oliet et al., 1997; Otani and Connor, 1998). These results suggest that, unlike glutamate, application of DHPG is not sufficient for PLC activation. In agreement, when endoplasmic reticulum (ER)-containing spines of CA1 neurons were stimulated at a low-frequency using glutamate uncaging, this induced group I mGluR-dependent LTD specific to the stimulated synapse and this LTD was dependent on Ca^{2+} release (Holbro et al., 2009).

2. mGluR-dependent LTD and neuronal output

The Long-term potentiation (LTP) and long-term depression (LTD) of synaptic transmission are considered memory-encoding mechanisms. LTP consists of two independent components: synaptic efficacy potentiation and excitatory postsynaptic potential (EPSP) to spike (E-S) potentiation, which is the increasing ability of an EPSP to generate a spike (Bear and Malenka, 1994; Bliss and Collingridge, 1993). The involvement of GABAergic mechanisms in E-S potentiation was recognized previously (Abraham et al., 1987; Chavez-Noriega et al., 1989; Chavez-Noriega et al., 1990), suggesting that activity-dependent suppression of inhibitory synapses, referred to as disinhibition, causes increased excitability and significantly influences the neuronal output. Indeed, the calcineurin-mediated inhibition of postsynaptic $GABA_A$ receptors (Lu et al., 2000) and the endocannabinoids (eCBs)-mediated inhibition of presynaptic GABA release (Chevaleyre and Castillo, 2003; Azad et al., 2004; Jiang et al., 2010) were shown to be involved in the inhibition of GABAergic synapses (i-LTD) to mediate increased excitability

associated with LTP in CA1 pyramidal neurons. However, the possibility that i-LTD is associated with LTD of excitatory synapses (e-LTD), especially mGluR-dependent e-LTD, has not been reported yet. It remains to be elucidated whether mGluR-dependent e-LTD is associated with E-S potentiation and, if it is, how the neuronal output is altered. Possibly, associated E-S coupling changes may be distinct in the two mGluR-dependent e-LTD types that recruit different signaling pathways.

3. Aim of this study

In this study, I have investigated in rat hippocampal neurons whether iGluRs play a significant role in mGluR-mediated PLC activation. Considering that PLC activity *per se* is dependent on intracellular Ca^{2+} concentrations (Ryu et al., 1987), the activation of iGluRs may contribute to group I mGluR-mediated PLC activation possibly by inducing Ca^{2+} influx directly or indirectly. The results of this study have shown that AMPA receptors initiate Ca^{2+} influx through L-type Ca^{2+} channels that is specifically required for mGluR-mediated PLC activation. Furthermore, I found evidence that this mechanism is crucial for mGluR-dependent e-LTD in the hippocampus

induced by paired-pulse low frequency synaptic stimulation (PP-LFS). I have also investigated whether PP-LFS-induced mGluR-dependent e-LTD is associated with E-S potentiation, and have effects on neuronal outcomes. The results of this study have shown that PP-LFS at SC pathway induced mGluR-dependent e-LTD, while the input–output (I–O) relationship paradoxically shifted leftward. I have provided evidence that PP-LFS activates an mGluR-dependent eCB signaling pathway, which leads to i-LTD, resulting in increased excitability and action potential (AP) output. By contrast, DHPG induces e-LTD without significant i-LTD, leading to no significant change in the I–O relationship. These results demonstrate that in hippocampal CA1 neurons the PP-LFS at SC pathway induces mGluR-dependent LTD at both excitatory and inhibitory synapses via signaling pathway involving postsynaptic located PLC, the outcome of which is in favor of excitation, resulting in a leftward shift in the I–O relationship.

MATERIALS AND METHODS

1. DNA constructs

The PLCδ-pleckstrin homology domain (PHδ) cloned into pEGFP-N1 was obtained from Dr. P. Suh (Ulsan National Institute of Science and Technology, Korea). The $Ca_v1.2$ (mouse) cloned into vector pcDNA6/V5-His was purchased from addgene (Plasmid 26572). The vector pcDNA6/V5-His containing $Ca_v1.3$ (rat) sequence that contains exon 42a was obtained from Dr. D. Lipscombe (Brown University, Providence, RI, USA). $Ca_v1.2$-targeting short-hairpin RNA (shRNA) sequence (5'-GCCGAAATTACTTCAATATTTCAAG AGAATATTGAAGTAATTTCGGC-3') was designed using the software tool available at the Whitehead Institute for Biomedical Research website (Yuan et al., 2004). The $Ca_v1.3$-targeting shRNA sequence (5'-GGAAACCATTTGACATATTTATTCAAGAGATAAATATGTCAAATGGT TTCC-3') was purchased from Open biosystems (UK). The synthesized $Ca_v1.2$ and $Ca_v1.3$ targeting shRNA oligonucleotides (CosmoGenetech,

Korea) were ligated into the lentiviral vector pLentiLox3.7 (pLL3.7) (Rubinson et al., 2003), which co-expressed monomeric RFP (mRFP). The pLL3.7 containing luciferase-targeting shRNA sequence (5`-TAAGGCTATGAAGAGATAC-3') was used as non-targeting control (NT control) (Dharmacon, Lafayette, CO, USA).

2. Cell culture and transfection

Neuron-glia co-culture protocol for low density hippocampal primary culture was previously described (Kaech and Banker, 2006; Lee et al., 2012). Briefly, hippocampi were dissected from embryonic day 18 Sprague Dawley (SD) rats of either sex. Hippocampal neurons were dissociated by papain treatment and trituration, and were plated at a density of 1.1×10^4 cells/cm^2 on poly-D-lysine (Sigma-Aldrich) coated coverslips (Marienfeld) in serum-based cell culture media. The next day, coverslips were transferred onto glial cell feeder layers cultured for 14 days in vitro (DIV14) in B-27 (Invitrogen)-supplemented Neurobasal A (Invitrogen) media. 5 μM 1-ß-D-cytosine-

arabinofuranoside (AraC, Sigma-Aldrich) was added to the DIV4 co-cultured neurons to prevent proliferation of glial cells. For western blotting experiments, hippocampal neurons were plated at a density of 4.4×10^4 cells/cm^2 on a poly-D-lysine coated culture dish. Primary cultured neurons (DIV4–7) were transfected using a calcium phosphate method (Ryan et al., 2005). The culture media were removed and saved before transfection. Neurons were incubated with fresh Neurobasal A media (2 ml per 60 mm culture dish) containing 25 mM HEPES (pH 7.35). During this time, the DNA/calcium phosphate precipitate was prepared by mixing one volume of PHδ-GFP DNA construct (1 μg) alone or with NT control, shCa_v1.2 or shCa_v1.3 DNA (5 μg for confocal imaging and Ca^{2+} measurement, 10 μg for western blotting) in 250 mM $CaCl_2$ with an equal volume of 2 × HBS (280 mM NaCl, 50 mM HEPES, 1.5 mM Na_2HPO_4, pH 7.1) using a vortex mixer. The precipitate was allowed to form for 2 min at room temperature (RT) before being added to the culture. 200 μl DNA/calcium phosphate suspensions were added drop-wise to cultured hippocampal neurons. A layer

of precipitate became obvious after a 15 min incubation period, when cells were quick-washed once and washed twice for 5 min interval with fresh Neurobasal A media and returned to the saved culture media.

HEK293 cells were plated at a density of 5×10^4 cells per 100 mm culture dish and maintained in DMEM (Invitrogen) supplemented with 10 % FBS and 1 % PS. HEK293 cells were sub-cultured before reaching ~80% confluence. HEK293 cells at ~30 % confluence were transfected as follows: 1) 5 μg $Ca_v1.2$ or 5 μg $Ca_v1.3$ alone 2) 5 μg $Ca_v1.2$ or 5 μg $Ca_v1.3$ with 5 μg NT control 3) 5 μg $Ca_v1.2$ or 5 μg $Ca_v1.3$ with 5 μg of $Ca_v1.2$ shRNA or $Ca_v1.3$ shRNA, respectively. This transfection was using the same calcium phosphate protocol for the primary culture except the medium was not changed before and after adding of DNA/calcium phosphate mixture to the culture. Cultures were maintained in a humidified incubator at 37 ˚C in 5 % CO_2.

3. Organitypic slice culture and Sindbis viral

transduction system

For slice cultures, P7-9 SD rats of either sex were decapitated and their brains were obtained. The posterior part of the brain was cut into 350 μm-thick transverse slices using a vibratome (ZERO 1; Dosaka, Kyoto, Japan) in ice-cold Eagle's balanced salt solution (EBSS) supplemented with 12.5 mM HEPES. The entorhino-hippocampi were dissected out and cultured using membrane interface techniques mostly according to a previously described procedure (De Simoni and Yu, 2006). Slices were placed on a porous (0.4 μm) membrane (Millicell-CM; Millipore) and fed with mixture of 50% MEM, 25% HS, 24% EBSS and 1% PS. Glucose was added to reach a final concentration of 36 mM. The media were changed to serum-free media (Neurobasal-A media with 2% B-27 supplement, 1% GlutaMAX-I, 1% PS and 5 mM glucose) with 5μM AraC the day after dissection. The media were changed every 2 d. We used a Sindbis virus system to overexpress PHδ-GFP in hippocampal organotypic slice cultures. PHδ-GFP was subcloned into SINrep (nsP2S726), a modified Sindbis viral vector that shows attenuated

viral-induced cytotoxicity and higher expression levels of the protein of interest in neurons (Kim et al., 2004). The complementary RNAs (cRNAs) were synthesized from the linearized SINrep (nsP2S726)/PHδ-GFP and helper DH-BB (tRNA/TE12) plasmid DNA, using in vitro transcription kit (mMessage mMachine, Ambion). BHK21 cells were electroporated with cRNAs of SINrep (nsP2S726)/PH-GFP and DH-BB (tRNA/TE12) according to Sindbis Expression System manual (Invitrogen). The pseudovirions-containing media were collected after 48 hrs, and then cell debris was removed from the supernatant by centrifugation at 1400 x g for 10 min at 4˚C and aliquots were stored at -80˚C. Subsequently, cultured hippocampal slices were infected at 8-15 DIV with titer resulting in infection of < 5% of neurons for 24 hrs.

4. Western blotting

Primary cultured hippocampal neurons or HEK293 cells were harvested after 7 days or 24 hrs of DNA transfection, respectively. The cells were washed

once with Dulbecco's phosphate-buffered saline (D-PBS) (Invitrogen) and solubilized in ice-cold lysis buffer containing 50 mM Tris-Cl (pH 7.4), 150 mM NaCl, 1 mM EDTA, 1% SDS and 0.1% protease inhibitor mixture (Sigma-Aldrich). Cell lysates were then sonicated 20 times at 1s interval and denaturated by 100℃ boiling water for 5 min. Cell lysates were clarified by centrifugation at 8200 × g for 1 min at 4℃. Cell lysates were separated by SDS-PAGE and transferred onto a polyvinylidene difluoride membrane (Millipore). The resulting blots were blocked for 1h in PBS plus 0.1% Triton X-100 (0.1% PBST) containing 5% skim milk (Difco). The blots were incubated overnight at 4℃ with specific primary antibodies: mouse monoclonal anti-$Ca_v1.2$ (1:150; Neuromab), rabbit polyclonal anti-$Ca_v1.3$ (1:100; alomone labs, Israel), goat polyclonal anti-$Ca_v1.3$ (1:100; Santa Cruz Biotechnology), or goat polyclonal anti-GAPDH (1:1500; Santa Cruz Biotechnology) as loading controls. The blots were washed with PBS containing 1% NP-40 and 0.1% SDS (washing buffer) for 1 hr and then twice with PBS for 30 min. After washing, the blots were incubated at room

temperature (RT) for 1h with the corresponding horseradish peroxidase-conjugated secondary antibodies: donkey anti-mouse IgG (1:2500; Jackson ImmunoResearch), donkey anti-rabbit IgG (1:2000; Abcam) or donkey anti-goat IgG (1:2000; Santa Cruz Biotechnology). The blots were then washed with washing buffer for 30 min and then twice with PBS for 15 min. Detection was performed using enhanced chemiluminescence reagent (GE Health-care Bioscience, UK) and exposed to x-ray films (Agfa Gevaert, Belgium).

5. Imaging and analysis of PHδ-GFP translocation

All images were obtained from DIV7-14 cultured neurons. Transfected cells were imaged with TCS-SP2 (Leica) confocal laser-scanning microscope using a 63× water-immersion objective (NA 1.20, HCX PL APO 63×, Leica) or FV300 (Olympus) using 63× water-immersion objective (NA 0.9, LUMPlanFl/IR, Olympus). Fluorochromes were excited with an argon laser at 488 nm and 543 nm. Appropriate emission filters were used for fluorescence

detection. PHδ-GFP favors phosphatidylinositol 4,5-bisphosphate (PIP_2) over phosphatidylinositol, phosphatidylinositol 3-phosphate, and phosphatidylinositol 3,4,5-triphosphate, but has approximately 10 times higher affinity for IP_3 than for PIP_2 (Varnai and Balla, 1998). Because of this affinity difference, PIP_2 hydrolysis by PLC causes PHδ-GFP to translocate from the plasma membrane to the cytosol. Dissociated hippocampal primary cultures were perfused with normal tyrode (NT) solution containing (mM): NaCl 150, KCl 5, $CaCl_2$ 2, $MgCl_2$ 1, glucose 10, HEPES 10, adjusted to pH 7.4 with Tris-OH while imaging. To make Ca^{2+}-free NT solutions, $CaCl_2$ was replaced by equimolar $MgCl_2$ and 0.1 mM EGTA was added. Organotypic hippocampal slice cultures were perfused with artificial cerebrospinal fluid (aCSF) containing (mM) : NaCl 124, $NaHCO_3$ 26, KCl 3.2, NaH_2PO_4 1.25, $CaCl_2$ 2.5, $MgCl_2$ 1.3, glucose 10, Na-pyruvate 3, vitamin C 3, bubbled with mixture of 95% O_2 and 5% CO_2 to a final pH of 7.4. To statistically analyze PHδ-GFP translocation, a region of interest (ROI)s were defined in the cytosol areas of soma or dendrite. Differences in the fluorescence intensity

(ΔF) inside ROI was obtained and normalized to baseline values (F_0) before 1st glutamate application (Fig. 1A-C, 2Ca, 2Cc, 4B, 4Cb). The relative ΔF values were calculated by normalizing ΔF to the peak values of 1st glutamate application (ΔF_1) (Fig. 3A-D, 5A-B). The $\Delta F_2/\Delta F_1$ values were obtained by calculating ratio between the ΔF induced by glutamate plus inhibitors (ΔF_2) and the ΔF induced by glutamate only (ΔF_1).

6. Calcium measurements in hippocampal primary neurons

DIV7-14 primary cultured hippocampal neurons were loaded by incubation with 2 μM Fura 2-AM plus 0.01 % Pluronic F-127 in NT solution for 10 min at RT then washed for 10 min to remove excess calcium indicators. For fluorescence excitation, I used a polychromatic light source (xenon-lamp based, Polychrome-IV; TILL-Photonics), which was coupled to the epi-illumination port of an inverted microscope (IX70, Olympus) via a quartz light guide and an UV condenser. Microfluorometry was performed with a

40× water immersion objective (NA 1.15, UAPO 40× W/340, Olympus) and a photodiode (TILL-Photonics). Standard two-wavelength protocol was used for fluorescence measurements of cells. Fluorescence intensity at an ROI including the soma was measured at 1 Hz with double wavelength excitation at 340 nm (F_{340}) and 380 nm (F_{380}). The ratio $R = F_{340}/F_{380}$ was converted to $[Ca^{2+}]_i$ values according to the following equation : $[Ca^{2+}]_i = K_{eff} (R - R_{min})/(R_{max} - R)$, where K_{eff} was estimated as 0.93 μM. Calibration parameters were determined by using *in vivo* calibration (Lee et al., 2000) and estimated R_{min} and R_{max} were typically 0.24 and 3.4, respectively.

7. Acute slice preparation

After decapitation, the whole brain was immediately removed and submerged in an ice-cold artificial cerebrospinal fluid (aCSF) containing (mM) NaCl 116, $NaHCO_3$ 26, KCl 3.2, NaH_2PO_4 1.25, $CaCl_2$ 0.5, $MgCl_2$ 7, glucose 10, Na-pyruvate 2, and vitamin C 3. Transverse hippocampal slices (300 μm thick) were prepared using a vibratome (VT1200S, Leica). Slices

were recovered at 32˚C for 30 min and then maintained at RT in an aCSF containing (mM) NaCl 124, $NaHCO_3$ 26, KCl 3.2, NaH_2PO_4 1.25, $CaCl_2$ 2.5, $MgCl_2$ 1.3, and glucose 10; I referred to the aCSFs as “recording aCSFs” until they were used for recordings. The recording aCSFs were used during electrophysiological recording. All aCSFs were bubbled with mixture of 95% O_2 and 5% CO_2 to a final pH of 7.4.

8. Electrophysiological recordings

Hippocampal CA1 pyramidal slices were transferred to an immersed recording chamber continuously perfused with oxygenated recording aCSF using a peristaltic pump (GILSON). CA1 pyramidal cells were visualized using an upright microscope equipped with differential interference contrast (DIC) optics (BX51WI, Olympus). All electrophysiological recordings were made in soma with an EPC-8 amplifier (HEKA Electronik) at a sampling rate of 10 kHz. Data recorded at different sampling rates are indicated. All the recordings were carried out at 32 ± 1˚C, and the aCSF perfusion rate was

maintained at 1−1.5 ml min^{-1}. Patch pipettes (3−4 MΩ) and monopolar stimulator pipettes (1−2 MΩ) were made from glass capillaries (Bo-glasscapollaries, Hilgenberg) using a puller (PC-10, Narishige). The pipettes were filled with internal solutions containing the following (mM): potassium gluconate 130, KCl 7, NaCl 2, $MgCl_2$ 1, EGTA 0.1, ATP-Mg 2, Na-GTP 0.3, and HEPES 10 (pH7.3 with KOH, 295 mosmol l^{-1} with sucrose). A stimulator (Stimulus Isolator A360; WPI) connected to a monopolar electrode filled with recording aCSF was placed in the stratum radiatum layer (horizontally and vertically ~120−150 μm away from the soma) of the CA1 field to evoke SC stimulation induced-synaptic responses. For excitatory postsynaptic current (EPSC) and inhibitory postsynaptic current (IPSC) recordings, the stimulator intensity (100 μs duration; 9−31.5 V) of extracellular stimulation was adjusted to evoke current amplitudes between 100 pA and 300 pA for the baseline. EPSCs and IPSCs were recorded from CA1 pyramidal neurons in a whole-cell configuration at a holding potential of −63 mV and +10 mV, respectively. I confirmed that EPSCs recorded at -

63 mV in the presence of APV were completely abolished by blocking AMPA receptors using NBQX, and that IPSCs recorded at +10 mV were completely abolished by blocking $GABA_A$ receptors using bicuculline. Immediately after whole-cell configuration, the pipette series resistance and capacitance were compensated manually and checked throughout the experiment. Cells in which the series resistance exceeded 20 MΩ and changed more than 15% during the experiment were discarded.

The mGluR-LTD was induced by PP-LFS (1 Hz, 15 min), and pharmacological mGluR-LTD was induced by DHPG application (7 min). The PP-LFS was performed in current-clamp mode at resting membrane potential (RMP) holding with the same stimulus intensity used for baseline EPSCs or IPSCs recordings. All recordings were performed in the presence of an NMDA receptor (NMDAR) antagonist (APV 50 μM) to block NMDAR-dependent LTD.

To measure tonic GABAergic currents, I applied voltage steps from the holding potential of −60 to −120 mV (5 ms duration) with a ten-second

interval, and plotted the changes in instantaneous currents measured at -60mV (I_{-60mV}) and -120 mV ($I_{-120\ mV}$) before I_h activation. The difference in $I_{-120\ mV}$ before and after GABA receptors (GABARs) antagonists was measured.

9. Drugs

AM-251, APV, bicuculline, CGP52432, CNQX, DHPG, LY367385, MPEP, NNC-711, picrotoxin, tetrodotoxin, ZD7288 and ω-Conotoxin MVIIC were purchased from Tocris (UK). U73122 was from Biomol. Fura 2-AM, EGTA-AM, and BAPTA-AM were from Molecular Probes. All other drugs were purchased from Sigma Aldrich. Stock solutions of these drugs were made by dissolution in de-ionized water or DMSO and were stored at -20℃. On the day of the experiment one aliquot was thawed and used. The concentration of DMSO in solutions was maintained below 0.1 %.

10. Statistical analysis

The data were analyzed using IgorPro (version 4.1, WaveMetrics) and OriginPro (version 8.0, Microcal) software and presented as mean ± SEM, where *n* represents the number of cells studied. The statistical significance of differences between the peaks was evaluated using a Student's *t*-test (paired) with confidence levels of $p < 0.01$ (**), $p < 0.05$ (*), and $p > 0.05$ (not significant, n.s.), and the precise *p* number is written in the results. Statistical correlations were tested using Pearson test.

RESULTS

1. Glutamate, but not DHPG, induces robust PLC activation in hippocampal neurons.

The intracellular signaling cascades elicited by DHPG application were independent of PLC in previous studies (Fitzjohn et al., 2001; Ireland and Abraham, 2002; Mockett et al., 2011; Schnabel et al., 1999; Sohn et al., 2007; Sohn et al., 2011). In addition, it is suspected that the apparent PLC-independence of mGluR-LTD may be due to the use of DHPG to induce LTD instead of more physiological methods (Luscher and Huber, 2010). Thus, the idea is tested that the ability to activate PLC may be different between DHPG and glutamate (the latter of which is released by fiber stimulation). To this end, green fluorescent protein (GFP)-labeled PLCδ-pleckstrin homology domain (PHδ-GFP) constructs were used to visualize PLC activation (Gamper et al., 2004; Horowitz et al., 2005).

Primary-cultured dissociated hippocampal neurons were transfected with PHδ-GFP construct, and confirmed preferential localization of fluorescent

signals at the plasma membrane (Single cell culture, “Control”) (Fig. 1Aa). Interestingly, the application of (*RS*)-3,5-DHPG (50 μM), a specific group I mGluR agonist, to the bath solutions did not induce discernable PHδ-GFP translocation (“DHPG ”, $\Delta F/F_0 = 0.02 \pm 0.01$, n = 19), whereas glutamate (30 μM) caused a robust translocation of PHδ-GFP into the cytosol (“Glu ”, $\Delta F/F_0 = 1.04 \pm 0.07$, n = 98, $p < 0.01$) (Fig. 1Aa, Ac). Line profiles of fluorescence intensity demonstrated that the cytosolic fluorescence, which reflects the generation of IP_3, remained unchanged with DHPG treatment, but was significantly increased by glutamate treatment (Fig. 1Aa, insets). To rule out the possibility that these observations are limited to dissociated hippocampal neurons, similar series of experiments were repeated in hippocampal slices. In organotypic slice culture systems, I confirmed that glutamate, but not DHPG, induced PHδ-GFP translocation (“DHPG”, $\Delta F/F_0 = 0.05 \pm 0.02$, n = 6 *vs* “Glu”, $\Delta F/F_0 = 0.57 \pm 0.13$, n = 7, $p < 0.01$) (Fig. 1Ab, Ac). Thus, results of this study suggest that stimulation of group I mGluR alone is not sufficient to activate PLC in hippocampal neurons.

2. Glutamate stimulates mGluR5 to activate PLC in hippocampal neurons.

Glutamate-induced translocation of PHδ-GFP was observed in multiple regions of the proximal dendrites (Fig. 1Ba, Bb), and these were not significantly different from those observed in the soma ("Soma", $\Delta F/F_0$ = 1.44 ± 0.24 *vs* "Dendrite", $\Delta F/F_0$ = 1.28 ± 0.21, n = 6, $p > 0.05$) (Fig. 1Bc). The increase in cytosolic fluorescence by glutamate was reliably repeated with similar magnitude when glutamate was re-applied after about 10 min interval ($\Delta F_2/\Delta F_1$ = 88.0 ± 3.6 %, n=10) (Fig. 1C, E). For some experiments, tetrodotoxin (TTX; 1 μM) was added in the bath solution prior to second glutamate application to block action potential-dependent events, and glutamate still induced reliable translocation of PHδ-GFP ($\Delta F_2/\Delta F_1$ = 83.6 ± 10.8%, n = 5, $p > 0.05$) (Fig. 1E). The glutamate-induced translocation of PHδ-GFP was significantly inhibited by PLC inhibitor U73122 (1 μM) ($\Delta F_2/\Delta F_1$ = 8.6 ± 3.1, n = 4, $p < 0.01$) (Fig. 1C, E) and 25 μM MPEP, a

specific mGluR5 blocker ($\Delta F_2/\Delta F_1$ = 11.2 ± 4.8%, n = 4, $p < 0.01$) (Fig. 1D , E), but it was not affected by LY367385 (100 μM), a specific mGluR1 blocker ($\Delta F_2/\Delta F_1$ = 84.1 ± 16.7%, n = 5, $p > 0.05$) (Fig. 1D, E). These results demonstrate that glutamate-induced translocation of PHδ-GFP is independent of action potential firing and occurs via the activation of mGluR5 and PLC.

3. Ca^{2+} influx via AMPA receptor activation is required for PLC activation by glutamate.

Given the differential effects of DHPG and glutamate, I suspected that glutamate may provide additional signaling mechanisms required for PLC activation via iGluRs. To test this idea, the contribution of iGluRs was examined using 10 μM CNQX or 50 μM APV, specific antagonists for AMPA receptors and NMDA receptors, respectively. As shown in Fig. 2Aa and 2Ac, glutamate-induced translocation of PHδ-GFP was blocked by CNQX ($\Delta F_2/\Delta F_1$ = 16.8 ± 4.2%, n = 5, $p < 0.01$), but it was not significantly

affected by APV ($\Delta F_2/\Delta F_1$ = 69.3 ± 8.0%, n = 5, $p > 0.05$). I also found that glutamate-induced translocation of PHδ-GFP was completely suppressed in Ca^{2+}-free bath solutions ($\Delta F_2/\Delta F_1$ = 9.0 ± 5.9%, n = 6, $p < 0.01$), but it was not significantly affected by 2 μM thapsigargin ($\Delta F_2/\Delta F_1$ = 89.6 ± 8.5%, n = 4, $p > 0.05$), which suggested a role of Ca^{2+} influx, but not Ca^{2+} mobilization (Fig. 2Ba, Bc). Thus, these results suggest that Ca^{2+} entry triggered by AMPA receptor activation may contribute to mGluR5-mediated PLC activation.

In a separate series of experiments, glutamate-induced Ca^{2+} transients ($[Ca^{2+}]_i$) were characterized to identify Ca^{2+} sources required for PLC activation by mGluR5 in primary-cultured dissociated hippocampal neurons loaded with 2 μM fura-2 AM. Bath applications of glutamate (30 μM) caused a rapid increase in $[Ca^{2+}]_i$ with an average amplitude of 438 ± 27 nM (n = 67). Glutamate-induced $[Ca^{2+}]_i$ increase was completely suppressed in Ca^{2+}-free bath solution ($[Ca^{2+}]_2/[Ca^{2+}]_1$ = 0.22 ± 0.1 %, n = 4, $p < 0.01$), but it was not affected by 2 μM thapsigargin ($[Ca^{2+}]_2/[Ca^{2+}]_1$ = 89.5 ± 8.5%, n =

4, $p > 0.05$) (Fig. 2Bb, Bc), indicating that glutamate-induced $[Ca^{2+}]_i$ increase is mostly mediated by Ca^{2+} influx, but not by Ca^{2+} release in cultured hippocampal neurons. I also confirmed that CNQX profoundly inhibits glutamate-induced $[Ca^{2+}]_i$ ($[Ca^{2+}]_2/[Ca^{2+}]_1 = 5.3 \pm 3.4\%$, n = 5, $p < 0.01$), but APV has no effect ($[Ca^{2+}]_2/[Ca^{2+}]_1 = 92.0 \pm 11.1\%$, n = 5, $p > 0.05$) (Fig. 2Ab, Ac). These results suggest that AMPA receptors, but not NMDA receptors, are largely responsible for the Ca^{2+} influx by glutamate. Given the calcium dependence of PLC activity (Rebecchi and Pentyala, 2000; Ryu et al., 1987), AMPA receptor-mediated depolarization and subsequent Ca^{2+} influx via voltage-gated Ca^{2+} channels (VGCCs) may facilitate PLC activation by mGluR5.

To test whether the opening of VGCCs independent of AMPA receptor stimulation can facilitate PLC activation by mGluR5, external K^+ concentration was elevated from 5 mM to 50 mM. The CNQX (10 μM) was added to the bath solution for these experiments so that the contribution of AMPA receptor-mediated depolarization by glutamate that is released from

presynaptic terminals in high K^+ conditions is excluded. Under this experimental condition, 50 mM KCl alone increased $[Ca^{2+}]_i$ to 697 ± 86 nM (n = 12), but had no effects on PHδ-GFP translocation ($\Delta F/F_0$ = 0.08 ± 0.03, n = 5) (Fig. 2Ca to Cc). When DHPG was added to 50 mM KCl, it robustly induced PHδ-GFP translocation ($\Delta F/F_0$ = 1.03 ± 0.2, n = 10, $p < 0.01$) (Fig. 2Ca, Cc). These findings further support that Ca^{2+} influx through VGCCs is required for PLC activation by mGluR5.

4. Both L-type and T-type Ca^{2+} channels mediate Ca^{2+} influx, but only L-type Ca^{2+} channels contribute to PLC activation.

I used specific Ca^{2+} channel blockers to identify specific Ca^{2+} channel subtypes that mediate Ca^{2+} influx and contribute to PLC activation. Glutamate-induced $[Ca^{2+}]_i$ is significantly inhibited when pretreated with nimodipine (10 μM), an L-type Ca^{2+} channel blocker ($[Ca^{2+}]_2/[Ca^{2+}]_1$ = 47.4 ± 10.1%, n = 7, $p < 0.01$) (Fig. 3A, E). Consistent with the effects on Ca^{2+}

influx, 10 μM nimodipine significantly blocked increase of cytosolic fluorescence ($\Delta F_2/\Delta F_1$ = 47.1 ± 7.9%, n = 5, $p < 0.01$) (Fig. 3A, E). A lower concentration (1 μM) of nimodipine inhibited $[Ca^{2+}]_i$ or PHδ-GFP translocation to a similar extent ($[Ca^{2+}]_2/[Ca^{2+}]_1$ = 44.1 ± 6.2 %, n = 7, $p < 0.01$; $\Delta F_2/\Delta F_1$ = 52.9 ± 7.9%, n = 5, $p < 0.01$). I also confirmed that 10 μM nimodipine significantly inhibits increase of cytosolic fluorescence in the proximal dendrite as well.

Mibefradil (5 μM), a T-type Ca^{2+} channel blocker, also significantly inhibited the glutamate-induced $[Ca^{2+}]_i$ ($[Ca^{2+}]_2/[Ca^{2+}]_1$ = 53.8 ± 3.0%, n = 9, $p < 0.01$) (Fig. 3B, E). In addition, simultaneous application of nimodipine (10 μM) and mibefradil (5 μM) had additive effect, inhibiting glutamate-induced $[Ca^{2+}]_i$ by ~75% ($[Ca^{2+}]_2/[Ca^{2+}]_1$ = 25.0 ± 5.3%, n = 5, $p < 0.01$). Interestingly, however, mibefradil did not inhibit glutamate-induced PHδ-GFP translocation ($\Delta F_2/\Delta F_1$ = 108.6 ± 24.8%, n = 6, $p > 0.05$) (Fig. 3B, E). Similar results were obtained with another T- type Ca^{2+} channel blocker, $NiCl_2$ (100 μM) ($[Ca^{2+}]_2/[Ca^{2+}]_1$ = 53.5 ± 4.4%, n = 5, $p < 0.01$; $\Delta F_2/\Delta F_1$ =

110.1 ± 22.4%, n = 5, $p > 0.05$) (Fig. 3E).

The amplitude of glutamate-induced $[Ca^{2+}]_i$ or PHδ-GFP translocation was not significantly affected by ω-conotoxin MVIIC (1 μM) ($[Ca^{2+}]_2/[Ca^{2+}]_1$ = 97.9 ± 6.6%, n = 5, $p > 0.05$; $\Delta F_2/\Delta F_1$ = 94.4 ± 6.3%, n = 5, $p > 0.05$), indicating that N-type and P/Q type Ca^{2+} channels are not involved (Fig. 3C, E). It was noted that 1-naphthyl acetyl spermine (NASPM, 10 μM), a specific Ca^{2+}-permeable AMPA blocker, slightly suppressed glutamate-induced $[Ca^{2+}]_i$ ($[Ca^{2+}]_2/[Ca^{2+}]_1$ = 80.0 ± 1.7%, n = 4, $p < 0.05$), but had no effect on PHδ-GFP translocation ($\Delta F_2/\Delta F_1$ = 84.9 ± 11.7%, n = 6, $p > 0.05$) (Fig. 3D, E).

I found that most of glutamate-induced Ca^{2+} influx is mediated by L-type and T-type Ca^{2+} channels, but Ca^{2+} influx through the L-type Ca^{2+} channels exclusively contribute to PLC activation by mGluR5 stimulation. Thus, the contribution of each Ca^{2+} source (L-type and T-type Ca^{2+} channels) to global Ca^{2+} transients is not proportional to its contribution to PLC activation (Fig. 3F). These findings suggest that PLC activation by glutamate is not

regulated by global Ca^{2+}, but by local Ca^{2+}. Therefore, it can be hypothesized that Ca^{2+} sensors involved in mGluR5-induced PLC activation is localized very closely to the L-type Ca^{2+} channels.

5. BAPTA , but not EGTA, inhibits PLC activation by glutamate significantly.

The coupling distance between Ca^{2+} sources and Ca^{2+} sensors is a key determinant of signaling properties, and it can be probed by comparing the effects of BAPTA and EGTA. BAPTA, a fast Ca^{2+} chelator, effectively captures the Ca^{2+} on its way from the Ca^{2+} channels to the Ca^{2+} sensors in a short distance (smaller than 100nm), whereas EGTA, a slow Ca^{2+} chela tor, selectively spares nanodomain Ca^{2+} signals (Eggermann and Jonas, 2012; Neher, 1998). Therefore, signal transmission is impaired by only BAPTA, but not by EGTA, when the coupling distance is short (nanodomain coupling), whereas both BAPTA and EGTA are effective when the coupling distance is longer (microdomain coupling). The same experimental approach

was used to probe the coupling distance between L-type Ca^{2+} channels and Ca^{2+} sensors involved in mGluR5-induced PLC activation. Firstly, I confirmed that the glutamate-induced increase in global Ca^{2+} was almost completely abolished in cultured hippocampal neurons loaded with BAPTA-AM (100 μM) or EGTA-AM (100 μM) for 30 min. Nonetheless, the glutamate-induced translocation of PHδ-GFP was significantly inhibited in BAPTA-loaded cells ($\Delta F_2/\Delta F_1$ = 45.4 ± 7.0%, n = 8, $p < 0.01$), but was not affected significantly in EGTA-loaded cells ($\Delta F_2/\Delta F_1$ = 69.3 ± 7.9%, n = 6, $p > 0.05$; $p < 0.05$ with BAPTA-loaded cells) supporting the nanodomain coupling between L-type Ca^{2+} channels and the Ca^{2+} sensors involved in PLC activation (Fig. 4A to C).

6. Both $Ca_v1.2$ and $Ca_v1.3$ contribute to PLC activation by glutamate.

$Ca_v1.2$ and $Ca_v1.3$ are the most widely expressed L-type Ca^{2+} channels in neurons (Hell et al., 1993). The RNA interference technique was employed

to determine the contribution of $Ca_v1.2$ and $Ca_v1.3$ Ca^{2+} channels to the glutamate-induced PHδ-GFP translocation (see *Materials and Methods*). Immunoblot analyses of HEK293 cells or primary cultured hippocampal neurons transfected with respective DNA constructs revealed that the expression of both $Ca_v1.2$ and $Ca_v1.3$ were significantly decreased by targeted short-hairpin RNAs (shRNAs) compared to non-targeted controls (NT control) (Fig. 5Aa, Ab).

Glutamate-induced $[Ca^{2+}]_i$ remained unchanged up to 7 days following transfection of primary-cultured dissociated hippocampal neurons with NT control, and the average $[Ca^{2+}]_i$ was 267.3 ± 30.4 nM (n=10) at 7 days post-transfection (dpt) (Fig. 5Ba, Ca). It was noted that glutamate-induced $[Ca^{2+}]_i$ in neurons transfected with $Ca_v1.2$-targeting shRNA ($shCa_v1.2$) were significantly decreased at 7 dpt ($[Ca^{2+}]_i$ = 99.7 ± 21.4, n = 14, $p < 0.01$) (Fig. 5Bb, Ca). In contrast, glutamate-induced $[Ca^{2+}]_i$ measured in neurons transfected with $Ca_v1.3$-targeting shRNA ($shCa_v1.3$) was slightly reduced, but not significantly different from those transfected with NT control ($[Ca^{2+}]_i$

= 215.0 ± 27.4, n = 8, $p > 0.05$) (Fig. 5Bc, Ca). These data suggest that $Ca_v1.2$ is the major isoform that mediates glutamate-induced Ca^{2+} influx.

Significant effects of $Ca_v1.2$ knockdown on glutamate-induced Ca^{2+} increase were observed after 5 dpt. Thus, the effects of $Ca_v1.2$ and $Ca_v1.3$ knockdown on glutamate-induced PHδ-GFP translocation were tested in neurons between 6 and 8 dpt. The normalized average amplitude ($\Delta F/F_0$) of the cytosolic fluorescence increment by glutamate in non-targeted cells was 0.55 ± 0.07 (n = 10), and it was significantly decreased to 0.15 ± 0.07 (n = 9, $p < 0.01$) in neurons transfected with sh$Ca_v1.2$ (Fig. 5Ba, Bb and Cb). The magnitude of inhibition by sh$Ca_v1.2$ for glutamate-induced PHδ-GFP translocation was comparable to that for glutamate-induced Ca^{2+} increase. Interestingly, glutamate-induced PHδ-GFP translocation was also significantly reduced by sh$Ca_v1.3$ ($\Delta F/F_0$ = 0.24 ± 0.06, n = 9, $p < 0.01$) (Fig. 5Bc, Cb). Finally, the effects of $Ca_v1.2$ and $Ca_v1.3$ knock-down on Ca^{2+} transients ($[Ca^{2+}]_i$ = 89.5 ±32.4, n = 9, $p < 0.01$) (Fig. 5Bd, Ca) and PHδ-GFP translocation ($\Delta F/F_0$ = 0.15 ± 0.05, n = 9, $p < 0.01$) (Fig. 5Bd, Cb) were

comparable to the effects of $Ca_v1.2$ knock-down alone.

7. mGluR-LTD is dependent on PLC and L-type Ca^{2+} channels at SC-CA1 pyramidal neuron excitatory synapse.

The results of this study indicate that DHPG is not sufficient to activate PLC in hippocampal neurons, which may serve as a clue to answer the question why mGluR-LTD induced by DHPG at excitatory synapses (e-LTD_{DHPG}) is independent of PLC, PKC, IP_3, and postsynaptic Ca^{2+} (Fitzjohn et al., 2001; Mockett et al., 2011; Schnabel et al., 1999). I confirmed that e-LTD_{DHPG} is not affected by the PLC inhibitor, U73122 ("Control", 59.9 ± 5.8 % of baseline at 40 min after 100 μM DHPG, n = 5 *vs* "U73122", 64.7 ± 3.7 % of baseline at 40 min after 100 μM DHPG in the presence of 10 μM U73122, n = 5, $p > 0.05$) (Fig. 6A).

It should be noted that mGluR-LTD induced by PP-LFS at excitatory synapses (e-$LTD_{PP\text{-}LFS}$) was demonstrated to involve PLC and PLC-

dependent signal pathways (e.g. PKC and postsynaptic Ca^{2+}) (Bolshakov and Siegelbaum, 1994; Holbro et al., 2009; Lee et al., 2005; Oliet et al., 1997; Otani and Connor, 1998; Reyes-Harde and Stanton, 1998). Possibly, PP-LFS to SC fibers induces Ca^{2+} channel activation associated with APs or dendritic Ca^{2+} spikes, thus contributing to PLC activation. To test this idea, the effects of blocking PLC or Ca^{2+} channels were examined on the changes of EPSCs amplitude induced by PP-LFS (1Hz for 15min) which consistently induces mGluR-LTD (Luscher and Huber, 2010). To inhibit NMDAR-dependent LTD, all recordings were performed in the presence of 50 μM APV. I confirmed that after PP-LFS to SC fibers, EPSCs amplitude was significantly reduced and this reduction lasted as long as the recording was maintained (52.4 ± 3.7 % of baseline at 35 min after PP-LFS, n = 8) (Fig. 6B-D). The $e\text{-}LTD_{PP\text{-}LFS}$ was prevented by 10 μM U73122 (98.2 ± 2.3 % of baseline at 35 min after PP-LFS, n = 6, $p < 0.01$) (Fig. 6B) and 25 μM MPEP (86.3 ±6.0 % of baseline at 35 min after PP-LFS, n = 6, $p < 0.01$) (Fig. 6C). The paird-pulse ratio (PPR) remained unchanged by $e\text{-}LTD_{DHPG}$ (“Control”,

150.4 ± 5.8 %; "LTD_{DHPG}", 157.8 ± 4.9 %, n = 5, $p > 0.05$) and e-$LTD_{PP\text{-}LFS}$ ("Control", 148.8 ± 5.0 %; "$LTD_{PP\text{-}LFS}$", 160.7 ± 9.7 %, n = 8, $p > 0.05$) (Fig. 6Ea, Eb). These findings demonstrate that mGluR-LTD induced by PP-LFS of SC axons onto the CA1 pyramidal neurons requires PLC activation.

Finally, I tested if L-type Ca^{2+} channels, which provide Ca^{2+} for PLC activation, are required for mGluR-LTD. I found that in the presence of 20 μM nimodipine PP-LFS to SC pathway did not induce LTD (92.0 ± 5.8 % of baseline at 35 min after PP-LFS, n = 7, $p < 0.01$) (Fig. 6D). Together, these findings demonstrate that mGluR-LTD at SC-CA1 synapses induced by PP-LFS involves PLC activation, and Ca^{2+} influx via L-type Ca^{2+} channels serves as a prerequisite.

8. E-S potentiation associated with $LTD_{PP\text{-}LFS}$ leads to increased AP output

The activation of group 1 mGluRs induces not only LTD (Kim et al., 2015; Luscher and Huber, 2010) but also increased excitability (Ireland and Abraham, 2002). To check whether the I–O relationship is affected during

mGluR-dependent e-LTD, several intrinsic parameters and E-S coupling that measured before PP-LFS induction (control) and 30min after LTD induction (pPP-LFS : post-PP-LFS) are compared (Fig. 7A). In accordance with EPSC depression, EPSP amplitudes were also reduced. In current clamp experiments, a burst synaptic stimulation (5 stimuli, 50 Hz, delivered every 2 s) was applied to record summated EPSPs (Fig. 7B). The amplitude of the 1st EPSP was significantly reduced after PP-LFS (0.56 ± 0.06, n = 8, p = 0.1), but the summation ratio (summated EPSP amplitude/1st EPSP amplitude) was unchanged (Control, 2.25 ± 0.2; pPP-LFS, 2.30 ± 0.4; n = 7, p = 0.9) (Fig. 7B). The decrement in EPSP amplitude after PP-LFS obtained from an individual cell was equivalent to that in its EPSC amplitude (Fig. 7C), suggesting that EPSP changes are parallel to EPSC changes, which indicates no significant change in dendritic excitability during e-LTD$_{PP-LFS}$. In the presence of the metabotropic glutamate receptor 5 (mGluR5) blocker MPEP (25 μM), EPSCs (1.00 ± 0.05, n = 7) and EPSPs (0.98 ± 0.08, n = 7) remained unchanged after PP-LFS, indicating that e-LTD$_{PP-LFS}$ is

predominantly mediated by mGluR5 (Fig. 7D). It is also confirmed that MPEP alone does not affect the basal synaptic transmission (EPSC amplitude: Control, 156.4 ± 16.0 pA; +MPEP, 152.1 ± 23.9 pA; n = 5, p = 0.7) or electrical properties such as RMP (Control, -58.1 ± 0.5 mV; +MPEP, -58.7 ± 0.5 mV; n = 6, p = 0.1) and R_{in} (Control, 136.7 ± 16.0 MΩ; +MPEP, 130.0 ± 17.6 MΩ; n = 6, p = 0.5).

Despite a significant decrease in EPSPs during e-$LTD_{PP\text{-}LFS}$, surprisingly, AP generation significantly increased after PP-LFS (Fig. 7E). I applied 10 burst stimulations at each stimulation intensity to measure the AP generation probability. Fig. 7E shows exemplary traces that were obtained at a stimulus intensity of 27 V before PP-LFS induction (Control) and 30 min after LTD induction (pPP-LFS). To plot I–O relationships, the stimulus intensity was varied in a wide range from subthreshold to suprathreshold and found that the I–O relationship shifted leftward after PP-LFS. The magnitude of the leftward shift after PP-LFS was quantified by comparing the stimulus intensity required for 50% AP probability (SI_{50}) in pPP-LFS with that in

Control (Fig. 7F). SI_{50} significantly decreased during e-$LTD_{PP\text{-}LFS}$ (SI_{50} = 0.78 ± 0.05 in pPP-LFS, n = 6, p = 0.02), and this decrease was abolished in the presence of MPEP (SI_{50} = 1.01 ± 0.06 in pPP-LFS, n = 7, p = 0.9) (Fig. 7F), suggesting that the leftward shift in the I–O relationship during e-$LTD_{PP\text{-}LFS}$ is dependent on mGluR5. The leftward shift in the I–O relationship despite synaptic depression may suggest the occurrence of E-S potentiation during e-$LTD_{PP\text{-}LFS}$. Therefore, the E-S curve was obtained by converting the x-axis into an EPSP slope (Fig. 7G). The EPSP slope to attain 50% AP probability (ES_{50}) after PP-LFS was 0.75 ± 0.03 (n = 6, p = 0.0006) of Control (Fig. 7G), indicating that PP-LFS induces a significant E-S potentiation.

The increase in AP firing probability at the same EPSP slope implies V_{th} changes during e-$LTD_{PP\text{-}LFS}$. I determined V_{th} as the membrane potential where dV/dt was over 10 V/s in the phase-plane plots and found that V_{th} was significantly hyperpolarized after PP-LFS (Control, −40.8 ± 0.8 mV; pPP-LFS, −46.0 ± 1.5 mV; n = 8, p = 0.0006) (Fig. 7H). These results suggest

that V_{th} hyperpolarization contributes to E-S potentiation during e-LTD_{PP-LFS}, which is powerful enough to induce a leftward shift in the I–O relationships despite synaptic depression.

9. The LTD of GABAergic synapses mediated by eCB underlies E-S potentiation during e-LTD_{PP-LFS}

The next question was the mechanism underlying E-S potentiation during e-LTD_{PP-LFS}. Disinhibition was suggested to participate in E-S potentiation during tetanus-induced LTP (Chavez-Noriega et al., 1989; Chavez-Noriega et al., 1990). To investigate whether disinhibition is involved in E-S potentiation during e-LTD_{PP-LFS}, I first examined whether IPSCs are reduced after PP-LFS. IPSCs evoked by stimulating the SC pathway were recorded at a holding potential of +10 mV. Changes of IPSCs after PP-LFS were monitored and found that the amplitude of IPSCs was reduced significantly after PP-LFS (0.38 ± 0.05 of baseline at 25–30 min after PP-LFS, n = 5) (Fig. 8A). Since the decrease in IPSCs persisted more than 30 min, I referred to it

as i-LTD. The IPSC amplitude reduction was accompanied by an increase in PPR (Control, 0.84 ± 0.06; 25–30 min after PP-LFS, 1.38 ± 0.3; n = 5, p = 0.04), suggesting that i-LTD is attributable to the decrease in GABA release from presynaptic terminals (Fig. 8A). Furthermore, I confirmed that i-LTD was abolished by MPEP (IPSC: 0.95 ± 0.09 of baseline at 25–30 min after PP-LFS; PPR: Control, 1.07 ± 0.09; 25–30 min after PP-LFS, 1.1 ± 0.08; n = 5, p = 0.3) (Fig. 8B). These results suggest that mGluR5-dependent mechanisms activated during PP-LFS affect presynaptic GABAergic terminals, possibly via retrograde signaling to cause i-LTD.

eCBs, such as 2-AG, have been suggested as retrograde signaling molecules to mediate high frequency stimulation-induced i-LTD in the CA1-SC synapse (Chevaleyre and Castillo, 2003, 2004; Younts et al., 2013). The activation of group 1 mGluRs triggers eCB mobilization upon PLC and diacylglycerol lipase α (DGLα) activation (Castillo et al., 2012). To assess a possible role of eCB signaling in i-LTD, I examined the effects of AM251, a type 1 cannabinoid receptor (CB_1R) antagonist, on i-LTD. In the presence of

AM251 (2 μM), PP-LFS no longer induced i-LTD, indicating that i-LTD depends on CB_1Rs (IPSC: 0.89 ± 0.08 of baseline at 25–30 min after PP-LFS; PPR: Control, 0.93 ± 0.1; 25–30 min after PP-LFS, 0.92 ± 0.1; n = 5, p = 0.9) (Fig. 8C). These results suggest that PP-LFS at the SC pathway activates mGluR5/PLC pathways in postsynaptic CA1 neurons, which mobilizes eCBs that activate CB_1Rs in presynaptic GABAergic interneuron terminals, resulting in reduced GABA release.

To further verify whether disinhibition indeed contributes to E-S potentiation, I examined if blocking GABARs can mimic the PP-LFS effects. When GABARs are blocked by applying a mixture of a $GABA_A$ receptor antagonist (bicuculline 20 μM or picrotoxin 100 μM) and a $GABA_B$ receptor antagonist (CGP52432 1 μM) (antiGABARs), the I–O relationship shifted leftward significantly (SI_{50} = 0.69 ± 0.03 with antiGABARs, n = 8, p = 0.00003) (Figs. 9A and 9B). However, the amplitude of EPSPs (Control, 3.7 ± 0.6 mV; +antiGABARs, 4.0 ± 0.8 mV; n = 8, p = 0.6) and the EPSP slope (Fig. 9C) were not significantly affected by antiGABARs, suggesting that

inhibitory postsynaptic potentials do not significantly affect EPSPs under the experimental conditions. Nevertheless, E-S coupling was significantly potentiated by antiGABARs (ES_{50} = 0.84 ± 0.03, n = 7, p = 0.002) (Fig. 9D), and this potentiation was associated with a significant V_{th} hyperpolarization (Control, −40.1 ± 1.0 mV; +antiGABARs, −42.2 ± 1.0 mV; n = 8, p = 0.0007) (Fig. 9E). On the other hand, significant changes were not observed when bicuculline was applied alone (SI_{50} = 1.01 ± 0.1 with bicuculline, n = 7, p = 0.9; V_{th} : Control, -41.3 ± 0.8 mV; +bicuculline, -41.8 ± 1.2 mV; n = 6, p = 0.6) or CGP52432 alone (SI_{50} = 1.06 ± 0.1 with CGP52432, n = 9, p = 0.6; V_{th} : Control, −40.5 ± 1.4 mV; +CGP52432, −40.8 ± 0.8 mV; n = 5, p = 0.9). These results suggest that both $GABA_A$ and $GABA_B$ receptors are required for E-S potentiation in CA1 neurons, and that V_{th} hyperpolarization is a major mechanism underlying E-S potentiation induced by disinhibition, which is consistent with the E-S potentiation mechanism by PP-LFS.

I then examined whether antiGABARs occlude PP-LFS effects. The antiGABARs did not affect the expression of e-$LTD_{PP\text{-}LFS}$ (0.61 ± 0.07 of

baseline at 25–30 min after PP-LFS, n = 6) (Fig. 9F) but inhibited the effects of PP-LFS on the I–O relationship or E-S coupling (Figs. 9G to 9I). In fact, AP generation decreased significantly after PP-LFS (SI_{50} = 1.21 ± 0.05 in pPP-LFS, n = 8, p = 0.003) (Fig. 9H), while E-S coupling (ES_{50} = 0.98 ± 0.02, n = 8, p = 0.4) (Fig. 9I) and V_{th} (+antiGABARs, −42.8 ± 1.3 mV; pPP-LFS, −43.9 ± 0.9 mV; n = 9, p = 0.3) (Fig. 9J) remained unchanged after PP-LFS in the presence of antiGABARs. The SI_{50} increase after PP-LFS in the presence of antiGABARs can be explained by a reduced EPSP amplitude with unchanged V_{th}. These results are consistent with the hypothesis that E-S potentiation associated with the V_{th} hyperpolarization after PP-LFS is attributable to disinhibition.

10. Reduction of tonic GABA currents underlies increased AP output with V_{th} hyperpolarization during e-$LTD_{PP\text{-}LFS}$

GABAergic inhibition is generally thought to occur via shunting effects. In

this regard, disinhibition that causes a reduction in shunting effects is expected to increase EPSPs, but it was noted that blocking GABARs does not increase the amplitude or slope of EPSPs (Fig. 9C). To understand this observation, disinhibition effects on R_{in} changes along with RMP changes were examined and found that antiGABARs did not significantly affect R_{in} (Control, 111.6 ± 8.4 MΩ; +antiGABARs, 117.7 ± 8.1 MΩ; n = 9, p = 0.1) (Fig. 10A) or RMP (Control, -59.4 ± 0.3 mV; +antiGABARs, -58.5 ± 0.8 mV; n = 9, p = 0.3). On the contrary, R_{in} was increased significantly after PP-LFS (Control, 117.7 ± 8.8 MΩ; pPP-LFS, 164.0 ± 14.2 MΩ; n = 8, p = 0.0005) (Fig. 10A), while RMP was unchanged (Control, −59.4 ± 0.6 mV; pPP-LFS, −60.1 ± 0.6 mV; n = 14, p = 0.2). However, PP-LFS-induced increases in R_{in} were unaffected by antiGABARs (+antiGABARs, 132.1 ± 8.1 MΩ; pPP-LFS, 164.1 ± 18.9 MΩ; n = 9, p = 0.05) (Fig. 10A), suggesting that disinhibition does not cause a significant increase in R_{in} and that the increased R_{in} after PP-LFS is not related to disinhibition.

Among PP-LFS induced effects and antiGABARs effects, V_{th}

hyperpolarization was commonly found and considered relevant as a mechanism for E-S potentiation. To further characterize the V_{th} change, V_{th} hyperpolarization for APs evoked by somatic depolarization was examined. APs were evoked by injecting depolarizing ramp currents (250 pA/s) to the soma under current clamp conditions, and the V_{th} for the first AP and the number of APs were measured before and 30 min after PP-LFS. After PP-LFS, V_{th} was hyperpolarized (Control, −41.4 ± 0.8 mV; pPP-LFS, −47.4 ± 1.9 mV; n = 6, p = 0.04) and more APs were evoked (Control, 8.7 ± 1.5; pPP-LFS, 12.3 ± 1.4; n = 6, p = 0.005) (Fig. 10B). The magnitude of V_{th} hyperpolarization for APs evoked by direct somatic stimulation was not significantly different from that evoked by SC stimulation (6.0 mV vs. 5.2 mV). The V_{th} values (Control, −39.8 ± 0.7 mV; pPP-LFS, −40.0 ± 2.0 mV; n = 6, p = 0.9) and AP numbers (Control, 7.7 ± 1.1; pPP-LFS, 7.3 ± 1.5; n = 6, p = 0.7) were unchanged after PP-LFS in the presence of MPEP (Fig. 10B), confirming the involvement of mGluR5 activation in these effects.

I then examined whether the inhibition of GABARs can mimic and

occlude PP-LFS effects. When antiGABARs were applied, the AP generation evoked by ramp current injection to the soma significantly increased (Control, 8.7 ± 2.0; +antiGABARs, 12.0 ± 1.6; n = 6, p = 0.03), and this increase was associated with a significant V_{th} hyperpolarization (Control, −40.4 ± 1.1 mV; +antiGABARs, −43.2 ± 1.5 mV; n = 6, p = 0.045) (Fig. 10C). Furthermore, in the presence of antiGABARs, PP-LFS did not affect AP generation (+antiGABARs, 10.7 ± 1.4; pPP-LFS, 11.0 ± 1.9; n = 9, p = 0.7) or V_{th} (+antiGABARs, −42.3 ± 1.4 mV; pPP-LFS, −43.0 ± 1.3 mV; n = 9, p = 0.5), indicating the occlusion of PP-LFS effects by antiGABARs (Fig. 10D). Applying $GABA_A$ or $GABA_B$ receptor antagonists alone did not show significant effects, suggesting the involvement of both $GABA_A$ and $GABA_B$ receptors in the increased AP firing associated with V_{th} hyperpolarization after PP-LFS.

A possible mechanism for the effects of antiGABARs and PP-LFS on APs evoked by somatic depolarization is that tonic GABA currents at an ambient GABA level have inhibitory roles for AP generation by increasing

V_{th}. Ambient GABA levels are expected to decrease when vesicular GABA release is reduced after PP-LFS, which in turn hyperpolarizes V_{th} and increases AP generation. To verify this hypothesis, identifying tonic GABA currents using the same internal solution used for AP recordings is a prerequisite. The conventional method for recording tonic GABA currents is to measure the change in holding current level by $GABA_A$ receptor antagonists under the condition that the driving force for Cl^- is maximized using a high Cl^- internal solution or ambient GABA concentration is maximized using GABA transporter inhibitors (Bright and Smart, 2013; Dalby, 2003; Glykys and Mody, 2007; Razik et al., 2013). Since detecting holding current level changes by applying antiGABARs was not successful with the low Cl^- internal solution used in the present study (calculated E_{Cl} −65.9 mV), I recorded changes in the current level by antiGABARs at −120 mV by applying voltage steps from the holding potential of −60 to −120 mV (5 ms duration) (Fig. 11A). Although $GABA_A$ or $GABA_B$ receptor antagonists alone did not induce significant changes, a small but significant

decrease in the current was observed when antiGABARs were applied. The different currents before and after applying antiGABARs recorded at −120 mV were regarded as GABARs-mediated currents (I_{GABARs}) (Control, −39.1 ± 8.0 pA, n = 9) (Figs. 11A and 11E). The current level at −120 mV was decreased by TTX (0.5 μM) (21.6 ± 5.3 pA, n = 5), and thus, the I_{GABARs} amplitude was reduced significantly in the presence of TTX (+TTX, −6.6 ± 4.5 pA, n = 5, p = 0.0008) (Figs. 11C and 11E). On the other hand, the current level at −120 mV was increased by NNC-711 (5 μM), a GABA uptake inhibitor (24.1 ± 9.3 pA, n = 7). The I_{GABARs} amplitude in the presence of NNC-711 was −46.2 ± 7.7 pA (n = 6) (Figs. 11D and 11E), slightly larger than that obtained from Control, although the difference was not statistically significant. These results support that I_{GABARs} is the current activated by ambient GABA. Importantly, antiGABARs had no effect on currents after PP-LFS, suggesting that I_{GABARs} became negligible after PP-LFS (pPP-LFS, −6.3 ± 2.5 pA, n = 7, p = 0.0003) (Figs. 11B and 11E). These results support that I_{GABARs} at the basal state, which has an inhibitory

role in the AP firing of CA1 neurons by V_{th} modulation, is reduced by PP-LFS, resulting in the AP firing increase during e-$LTD_{PP\text{-}LFS}$.

11. The PP-LFS-induced reduction of tonic inhibition is mediated by eCB/CB_1R activation

I have shown that i-LTD is mediated by eCB/CB_1Rs (Fig. 8C). Considering that the main source of ambient GABA responsible for tonic inhibition in the hippocampus is the vesicular GABA release responsible for activating phasic inhibition (Glykys and Mody, 2007), I examined whether eCB/CB_1R activation is involved in the reduction of tonic currents after PP-LFS. In the presence of AM251, I_{GABARs} was well detected after PP-LFS, and no significant difference was determined between the I_{GABARs} amplitudes obtained before and after PP-LFS (no PP-LFS, −22.3 ± 2.6 pA at −120 mV, n = 6; pPP-LFS, −20.8 ± 1.2 pA at −120 mV, n = 5; p = 0.6) (Figs. 12A to 12C). In agreement of this finding, PP-LFS-induced V_{th} hyperpolarization was abolished in the presence of AM251 (V_{th}_ramp: +AM251, −39.0 ± 0.4

mV; pPP-LFS, −40.4 ± 0.4 mV; n = 9, p = 0.1; V_{th}_SC: +AM251, −39.8 ± 0.7 mV; pPP-LFS, −40.8 ± 0.6 mV; n = 6, p = 0.2) (Figs. 12D and 12E). Collectively, these results suggest that the PP-LFS-induced increases in somatic excitability and E-S potentiation are mediated by the CB_1R-dependent inhibition of the inhibitory input.

12. DHPG does not induce the leftward shift in I–O relationship during e-LTD

Next, I investigated whether mGluR-LTD at excitatory synapses induced by the group 1 mGluR agonist DHPG (e-LTD_{DHPG}) also leads to a leftward shift in I–O relationship and E-S coupling. As were the changes during e-LTD_{PP-LFS}, EPSC changes during e-LTD_{DHPG} were parallel to EPSP changes (0.71 ± 0.06, n = 7) (Fig. 13A). However, the I–O relationship during e-LTD_{DHPG} was different from that during e-LTD_{PP-LFS} (Figs. 13B and 13C). The AP output during e-LTD_{DHPG} in response to burst synaptic stimulation was not consistently increased or decreased but showed a variable response. As a

result, the mean value for SI_{50} during e-LTD_{DHPG} was not significantly different from that obtained before DHPG application (SI_{50} = 1.02 ± 0.08, n = 11, p = 0.9) (Fig. 13C). To understand the I–O response variability during e-LTD_{DHPG}, the magnitudes of output changes (1 - normalized SI_{50}) and synaptic weight changes ($EPSP_{DHPG}/EPSP_{Control}$) were compared and found a linear relationship between these two parameters (Fig. 13C), suggesting that synaptic weight is a major factor for determining AP outputs. Interestingly, the relationship crosses zero when EPSPs were reduced by about 20%, suggesting that 20% of the EPSP reduction was compensated by another mechanism that increases excitability. The analysis of the E-S coupling revealed a somewhat variable response in that most cells showed E-S potentiation while a few cells showed E-S depression. The mean value for ES_{50} decreased significantly after DHPG (ES_{50}, 0.93 ± 0.03, n = 10, p = 0.01) (Fig. 13D), but the decrease was smaller than that observed after PP-LFS. To examine the involvement of i-LTD in DHPG-induced E-S potentiation, changes in IPSCs after DHPG (0.82 ± 0.06 of baseline at 25–30 min after

DHPG, n = 10) were measured (Fig. 13E). In contrast to the expression of significant i-LTD after PP-LFS, only three out of ten cells showed IPSC decreases after DHPG by more than 20% (indicated by a box, Fig. 13F). There was no correlation between the magnitudes of i-LTD and E-S potentiation (Fig. 13F) or V_{th} changes (Fig. 13G: number indicates 3 cells that show significant i-LTD in Fig. 13F), suggesting that the increased excitability underlying E-S potentiation during e-LTD_{DHPG} is not mediated by disinhibition (Fig. 13F). The V_{th} showed variable responses with no significant change in the mean value for V_{th} after DHPG (Control, −41.0 ± 0.6 mV; pDHPG, −41.5 ± 2.0 mV; n = 11, p = 0.4), but the V_{th} changes of individual cells correlated with E-S coupling changes after DHPG (Fig. 13G). A correlation between E-S coupling changes and R_{in} changes was not observed (Fig. 13H). These results suggest that the E-S coupling changes after DHPG involve an intrinsic plasticity mechanism that regulates V_{th}. Considering that V_{th} hyperpolarization by antiGABARs (2.1 mV) was smaller than that by PP-LFS (5.2 mV), intrinsic plasticity mechanisms may

also be involved in PP-LFS effects.

13. No evidence for the involvement of I_h inhibition in the increased excitability during mGluR-dependent LTD

Increased excitability due to I_h downregulation during mGluR-dependent LTD was reported previously (Brager and Johnston, 2007). To investigate the involvement of I_h inhibition in the increased excitability during e-LTD_{PP-LFS}, excitability parameter changes induced by I_h blockade using ZD7288 (20 μM) were analyzed and compared them with changes induced by PP-LFS. I confirmed that three typical features for I_h inhibition (Biel et al., 2009; Maccaferri et al., 1993)—RMP hyperpolarization (Control, -58.8mV ± 0.8 mV; +ZD7288, −67.5 ± 1.7 mV; n = 9, p = 0.0003), R_{in} increase (Control, 131.3 ± 11.1 MΩ; +ZD7288, 250.0 ± 34.6 MΩ; n = 5, p = 0.01), and sagging amplitude decrease (Fig. 14A)—were well observed in the presence of ZD7288, while PP-LFS did not significantly affect RMP or sagging (Fig.

14B). Increased R_{in} due to I_h inhibition is expected to increase EPSP decay time and temporal summation (Brager and Johnston, 2007; Magee, 1999), but the summation ratio for EPSPs in response to 50 Hz burst synaptic stimulation was not affected by ZD7288 (Control, 2.73 ± 0.3; +ZD7288, 2.80 ± 0.3; n = 6, p = 0.8) (Fig. 14C). As a result, the I–O relationship obtained from APs evoked by synaptic stimulation was shifted rightward by ZD7288 (SI_{50}, 1.65 ± 0.1, n = 5, p = 0.01) (Fig. 14D) with no significant changes in V_{th} (Control, −38.0 ± 1.4 mV; +ZD7288, −36.0 ± 1.9 mV; n = 5, p = 0.09) (Fig. 14E). These results showed that I_h inhibition effects on intrinsic excitability and E-S coupling are quite different from PP-LFS effects. I also analyzed excitability changes during e-LTD_{DHPG} and found no significant changes in RMP (Control, -59.5 ± 0.4 mV; pDHPG, -61.0 ± 0.9 mV; n = 14, p = 0.1), R_{in} (Control, 159.0 ± 3.8 MΩ; pDHPG, 173.9 ± 8.5 MΩ; n = 10, p = 0.2), or sagging, which is also very different from I_h inhibition effects. The effects of ZD7288 on intrinsic excitability were further investigated by analyzing AP firing in response to somatic

depolarization. The number of spikes induced by somatic depolarization was reduced by ZD7288 (100 pA injection; Control, 4.4 ± 1.3; +ZD7288, 2.9 ± 1.1, n = 8, p = 0.01), but the reduction was reversed when the hyperpolarized RMP was corrected by current injection (+ZD7288 (RMP corrected), 8.3 ± 1.7, n = 8, p = 0.05) (Fig. 14F), suggesting that the increased excitability due to R_{in} increase was masked by RMP hyperpolarization effects. Importantly, V_{th} was not affected by ZD7288 (Control, −38.6 ± 0.6 mV; +ZD7288, −36.6 ± 2.5 mV, n = 5, p = 0.4) or changing RMP (+ZD7288 (RMP corrected), −36.4 ± 2.6 mV, n = 5, p = 0.3) (Fig. 14G), suggesting that V_{th} hyperpolarization, which is the most important mechanism for E-S potentiation during e-LTD, is not attributable to I_h inhibition.

14. PP-LFS-induced leftward shift in I-O relationship at perforant pathway-CA1 synapse is independent of i-LTD

It is well known that CA1 pyramidal neurons receive two major excitatory

inputs, one from hippocampal CA3 and another from entorhinal cortex which is named as perforant pathway. It has been demonstrated perforant pathway-CA1 synapses also express LTD by LFS (Xu et al., 2010). I asked whether E-S potentiation or depression is associated with LTD at perforant pathway-CA1 synapses and if so plasticity i-LTD plays a role. While LTD was expressed by PP-LFS at perforant pathway-CA1 synapses, the magnitude was lower than SC-CA1 LTD (72.9 ± 13.1 % of baseline at 25 min to 30 min after PP-LFS, n = 7, Fig. 15A), which is consistent with the previous study (Xu et al., 2010). Next, I checked changes in I-O relationships at perforant pathway-CA1 synapse. As changes observed at SC-CA1 synapse, leftward shift of I-O relationship (pPP-LFS (PP), SI_{50} = 0.77 ± 0.08; n = 5; $p < 0.05$) (Fig. 15B and 15D) and V_{th} hyperpolariation (V_{th}_ramp : Control, -38.9 ± 1.4 mV; pPP-LFS (PP), -45.2 ± 1.8 mV; n = 5; $p < 0.05$; V_{th}_PP : Control, -40.1 ± 1.2 mV; pPP-LFS (PP), -46.4 ± 1.7 mV; n = 5; $p < 0.05$) were equally expressed at perforant pathway-CA1 synapse (Fig. 15E, 15G, 15H, and 15J). However, R_i (Control, 145.4 ± 20.7 MΩ;

pPP-LFS (PP), 153.7 ± 21.4 MΩ; n = 5; $p > 0.05$) and sagging were not significantly changed by PP-LFS. To examine whether PP-LFS induced leftward shift in I-O relationship at distal dendrites of CA1 neuron is mediated by disinhibition, I performed same protocols in the presence of antiGABARs. Although LTD was still expressed during blocking inhibitory inputs (82.6 ± 2.4 % of baseline at 25 min to 30min after PP-LFS, n = 6) (Fig. 15A), unlike stimulating SC, V_{th} (V_{th}_ramp : Control, -41.5 ± 1.1 mV; pPP-LFS, -46.1 ± 1.9 mV; n = 5; $p < 0.05$; V_{th}_PP : Control, -41.8 ± 0.8 mV; pPP-LFS, -45.0 ± 0.5 mV; n = 5; $p < 0.05$) (Figs. 15F, 15G, 15I and 15J) and I-O relationships (pPP-LFS (PP), SI_{50} = 0.85 ± 0.05; n = 6; $p < 0.05$) (Figs. 15C and 15D) were still significantly changed while inhibitory inputs were blocked at perforant pathway-CA1 synapses. Together, these results indicate that PP-LFS-induced disinhibition is limited to SC-CA1 synapse, not perforant pathway-CA1 synapses.

DISCUSSION

This study demonstrates that the importance of AMPA receptor-initiated Ca^{2+} influx via L-type Ca^{2+} channels in PLC activation by mGluR5 in hippocampal neurons. I also confirmed that hippocampal mGluR-LTD, induced by the stimulation of SC fibers, is dependent on PLC. This study proposes that glutamate activates both AMPA and mGluRs, and their downstream events interact with each other to ensure reliable PLC activation in physiological conditions. I further demonstrated that the sustained and stable activation of mGluR5 by SC fibers stimulation induces not only mGluR-dependent e-LTD, but also i-LTD resulting in an E-S potentiation in CA1 pyramidal neurons. This opposite expression of synaptic and E-S coupling plasticity leads to increased neuronal output, implying that E-S coupling alteration is not just a complementary mechanism to synaptic plasticity but can play a dominant role in regulating the I–O relationship. Fig. 16 summarizes the data for alterations of synaptic weights, E-S coupling, and I–O relationship, demonstrating that I–O relationship alterations,

referred to as I–O plasticity, during mGluR-LTD can be understood by the integration of changes in synaptic and E-S coupling components.

1. Local Ca^{2+}-dependence of mGluR5-mediated PLC activation

Ca^{2+} dependence of PLC activation by group I mGluRs and muscarinic receptors was previously reported (Hashimotodani et al., 2005; Maejima et al., 2005; Masgrau et al., 2000; Masgrau et al., 2001). In cerebellar granule cells, activation of PLC by glutamate, which is mediated by mGluR1, was dependent on the external Ca^{2+} (Masgrau et al., 2001), whereas muscarinic receptor-mediated activation of PLC was modulated by changes in the loading state of intracellular Ca^{2+} store (Masgrau et al., 2000). These results suggest that the Ca^{2+} source facilitating PLC activation is specific to each receptor. Notably, these results are consistent with the idea that receptor-mediated PLC activation is regulated by local Ca^{2+}. However, the specific Ca^{2+} source to induce local Ca^{2+} increase remained unclear. In the present

study, the involvement of Ca^{2+} stores was excluded in glutamate-induced PLC activation by showing that thapsigargin affected neither glutamate-induced $[Ca^{2+}]_i$ increase nor PHδ-GFP translocation (Fig. 2). From the effects of Ca^{2+} removal, I confirmed the role of Ca^{2+} influx in glutamate-induced $[Ca^{2+}]_i$ increase and PLC activation, and investigated the involvement of specific Ca^{2+} influx pathways. Both L-type and T-type Ca^{2+} currents contribute similarly to glutamate-induced Ca^{2+} influx (Fig. 3), which is consistent with previous studies showing abundant expression of L-type ($Ca_v1.2$ and $Ca_v1.3$) and T-type ($Ca_v3.1$, $Ca_v3.2$ and $Ca_v3.3$) Ca^{2+} channels in the soma and proximal dendrites of hippocampal neurons (Leitch et al., 2009; McKay et al., 2006), whereas only L-type Ca^{2+} channels contribute to PLC activation (Fig. 3, 4). The discrepancy between the contribution of each Ca^{2+} channel to global Ca^{2+} and its contribution to PLC activation supports the local Ca^{2+}-dependence of mGluR5-mediated PLC activation in hippocampal neurons. In addition, BAPTA is more effective than EGTA at inhibiting mGluR-mediated PLC activation (Fig. 5), which

confirms the nanodomain coupling between L-type Ca^{2+} channels and Ca^{2+} sensors involved in PLC activation. It needs to be noted that both glutamate-induced Ca^{2+} increases and PHδ-GHP translocation were abolished completely in Ca^{2+}-free, but the inhibition of L-type Ca^{2+} channels did not induce complete abolishment. These results suggest the presence of another Ca^{2+} entry pathway that couples to PLC activation, but I could not identify the nature of this pathway in the present study.

Among members of L-type Ca^{2+} channel subfamily ($Ca_v1.1$ to $Ca_v1.4$), $Ca_v1.2$ and $Ca_v1.3$ channels are expressed in neurons. They are often present in the same cell, but accumulating evidence shows that they play differential roles (Berger and Bartsch, 2014). Since there are no pharmacological drugs that are selective for either $Ca_v1.2$ or $Ca_v1.3$ isoform, sh-RNA for each isoform was used to investigate whether the specific L-type Ca^{2+} channel subunits provide local Ca^{2+} for PLC activation by mGluR5 (Fig. 5). Inhibitition of Ca^{2+} response by sh$Ca_v1.2$ was large (63% reduction) and significant, while the effect of sh$Ca_v1.3$ was insignificant. The effect of

knockdown of both subunits is not different from the effect of sh$Ca_v1.2$ alone, suggesting that $Ca_v1.2$ is the major isoform that mediates L-type Ca^{2+} currents. Furthermore, inhibition of PHδ-GFP translocation by sh$Ca_v1.2$ (73% reduction) was comparable to its effect on Ca^{2+} response, supporting the idea that close coupling between $Ca_v1.2$ and PLC underlies the observed Ca^{2+}-dependence of glutamate-induced PLC activation. A recent study showing that mGluR5 physically interacts with $Ca_v1.2$ subunits in hippocampal neurons (Kato et al., 2012) is consistent with this idea. It was surprising, however, to find that sh$Ca_v1.3$, which showed little effect on Ca^{2+} response, significantly inhibited glutamate-induced PHδ-GFP translocation (55% reduction), suggesting a significant role of $Ca_v1.3$ in PLC activation. However, the effect of sh$Ca_v1.3$ on PHδ-GFP translocation was not additive to the effect of sh$Ca_v1.2$ in double knockdown experiments. These results may suggest that $Ca_v1.3$ is involved in glutamate-induced PLC activation, but not as a Ca^{2+} source. I do not have a clue for the molecular mechanism for Ca^{2+}-independent mechanism of $Ca_v1.3$, but such possibility needs to be

elucidated in future studies. I could not entirely exclude some off-target effects of shCa$_V$1.3.

2. Reduced tonic GABA currents, the main mechanism for E-S potentiation by PP-LFS at SC-CA1 synapses

The increase in intrinsic excitability during e-LTD has been demonstrated previously (Brager and Johnston, 2007; Campanac et al., 2008; Gasselin et al., 2017). Increases in AP firing during e-LTD were associated with R_{in} increases (Brager and Johnston, 2007), and R_{in} changes correlated closely with the magnitude of LTD (Gasselin et al., 2017). The increase in EPSP decay time caused by R_{in} increases was suggested to cause an increase in EPSP summation (Brager and Johnston, 2007). Based on these reports, the R_{in} increase is considered as an indication of an increase in intrinsic excitability during e-LTD, but direct experiments to show whether it contributes to E-S potentiation have not been conducted. In fact, increases in EPSP summation were observed at frequencies lower than 20 Hz (Brager

and Johnston, 2007), but I used burst synaptic stimulation at 50 Hz to evoke APs with mild stimulation. Under this condition, the temporal summation of EPSPs was not affected by PP-LFS (Fig. 7B), suggesting that the R_{in} increase may not contribute to E-S potentiation. I searched for another mechanism underlying E-S potentiation changes during e-LTD and found that it has a strong correlation with V_{th} hyperpolarization (Figs. 7 and 9).

I demonstrate that antiGABARs mimic and occlude PP-LFS effects on E-S potentiation and V_{th} without significant effects on R_{in} (Figs. 9 and 10), supporting the idea that disinhibition is responsible for V_{th} hyperpolarization and serves as a key mechanism underlying E-S potentiation during e-LTD_{PP-LFS}, while R_{in} increases play a minor role in our experimental condition. However, this study does not exclude the possible contribution of intrinsic plasticity to E-S potentiation during e-LTD_{PP-LFS}. The E-S potentiation and V_{th} hyperpolarization induced by antiGABARs were, in fact, smaller than those induced by PP-LFS (ES_{50}, 75% after PP-LFS vs. 84% after antiGABARs; V_{th} hyperpolarization, 5.2 mV after PP-LFS vs. 2.1 mV after

antiGABARs). Furthermore, E-S potentiation associated with V_{th} hyperpolarization also occurred during e-LTD_{DHPG} where i-LTD was insignificant (Fig. 13), though the magnitude was smaller than that during e-$LTD_{PP\text{-}LFS}$. These results may suggest that intrinsic excitability changes independent of the GABAergic mechanism also contribute to E-S potentiation during e-LTD.

I_h inhibition is well-known as a mechanism for an increased intrinsic excitability (Brager and Johnston, 2007; Gasselin et al., 2017). Increased R_{in} by ZD7288 is accompanied by a huge RMP hyperpolarization (Fig. 14), while increased R_{in} during e-$LTD_{PP\text{-}LFS}$ is not accompanied by RMP changes. Furthermore, sagging, a manifestation of I_h activation, was not significantly affected by PP-LFS (Fig. 14B). These differences between I_h inhibition effects and PP-LFS effects suggest that I_h inhibition may not contribute significantly to intrinsic excitability changes. In the present study, I could not identify ion channels that cause increased excitability, but the results suggest that changes in ion channel activity leading to V_{th} hyperpolarization are most

likely to contribute to increased excitability.

The main source of ambient GABA responsible for tonic inhibitory currents in the hippocampus is the vesicular release responsible for phasic inhibition (Glykys and Mody, 2007). The contribution of reduced tonic inhibition to tetanus-induced E-S potentiation was suggested previously (Chavez-Noriega et al., 1990), but the relative contribution of phasic and tonic inhibition has not been investigated. I found that PP-LFS-induced V_{th} hyperpolarization to synaptic stimulation (Fig. 13F) is similar to direct somatic activation (Fig. 16B) and that both changes are occluded by antiGABARs (Figs. 15J and 16D). These results suggest that the reduction of tonic inhibitory currents is mainly responsible for V_{th} hyperpolarization and E-S potentiation during e-$LTD_{PP\text{-}LFS}$.

It is generally understood that the mechanism causing excitability increases via disinhibition is a reduction in shunting effects, which is expected to increase R_{in} and EPSP amplitude. However, when I calculated

from our experimental results the contribution of tonic GABA conductance to resting conductance (-39 pA at -120 mV with E_{Cl} = -66 mV), it was only about 8% (0.7 nS out of 9 nS). In fact, significant changes in R_{in} and EPSP amplitude were not found by antiGABARs, but the mean value for R_{in} increased by 5.5% (from 111 MΩ to 117 MΩ), which is not greatly different from the value expected from a conductance change by a reduction in tonic GABA currents. Despite a minor effect of tonic GABA currents on the whole cell conductance, tonic GABA currents have a great influence on AP output by hyperpolarizing V_{th}. One possible explanation for these findings is that the shunting effect of tonic GABA currents is not global but specifically coupled to Na^+ channels. This needs to be investigated in future studies.

It was reported that tonic inhibitory currents in the CA1 area are mostly mediated by $GABA_A$ receptors (Glykys and Mody, 2006, 2007; Stell and Mody, 2002). However, applying $GABA_A$ or $GABA_B$ receptors antagonists individually did neither significantly affect V_{th} and E-S potentiation nor occlude PP-LFS effects, suggesting that not only $GABA_A$ receptors but also

$GABA_B$ receptors underlie the tonic inhibition. $GABA_B$ receptor-mediated tonic inhibition was reported in locus coeruleus neurons, playing a role in the regulation of spontaneous activity (Wang et al., 2015). An enhancement of $GABA_A$ receptor function by postsynaptic $GABA_B$ receptors was reported in dentate gyrus granule cells (Ransom et al., 2013) and thalamocortical neurons (Connelly et al., 2013). The roles for $GABA_B$ receptors in the tonic inhibition in CA1 neurons remain to be investigated.

CA1 neurons also receive a direct sensory input from entorhinal cortex layer III neurons through perforant pathway. Unlike SC-CA1 syanseps, i provide the evidence that the V_{th} hyperpolarization and leftward shift in I-O relationship during PP-LFS induced LTD in perforant pathway-CA1 synapses was not dependent on inhibitory inputs and this results indicate that there is a possibility of an another mechanism for regulating I-O relationship at this synapse. This study highlights the mechanisms underlying the activity-dependent regulation of the I-O relationship that specific to SC-CA1 syanpses, which may play an important role in information processing in the

hippocampus.

3. Difference in signaling mechanism underlying e-LTD$_{PP-LFS}$ and e-LTD$_{DHPG}$

It is well-established that mGluR-LTD in the cerebellum is dependent on PLC activation (Kano et al., 2008). Cerebellar mGluR-LTD requires both parallel fiber stimulation and the depolarization of Purkinje cell (postsynaptic) membranes (Kano et al., 2008). Likewise, when hippocampal e-LTD$_{PP-LFS}$ was induced (i.e. when released glutamate depolarizes the postsynaptic membrane via AMPA receptors), mGluR-LTD consistently required postsynaptic Ca^{2+} (either Ca^{2+} mobilization or Ca^{2+} influx), PKC, and PLC (Bolshakov and Siegelbaum, 1994; Holbro et al., 2009; Lee et al., 2005; Oliet et al., 1997; Otani and Connor, 1998; Reyes-Harde and Stanton, 1998). In contrast, e-LTD$_{DHPG}$ was found to be independent of postsynaptic Ca^{2+}, PKC, and PLC (Fitzjohn et al., 2001; Mockett et al., 2011; Schnabel et al., 1999). Furthermore, considering that PLC is required for the DAG

generation, which is a prerequisite to generating endocannabinoids such as 2-AG that is crucial for presynaptic expressing CB_1R and subsequent protein synthesis-dependent i-LTD (Castillo, 2012; Edwards et al., 2008; Heifets and Castillo, 2009; Younts et al., 2016), the failure of i-LTD induction by DHPG is consistent with that mGluRs activation alone is insufficient to activate PLC (Figs. 13 and 16). Therefore, I suggest that mGluR-LTD in physiological conditions requires PLC while chemical LTD (LTD_{DHPG}) may bypass PLC activation and use alternative signaling pathways that resulting different impacts on I-O relationship.

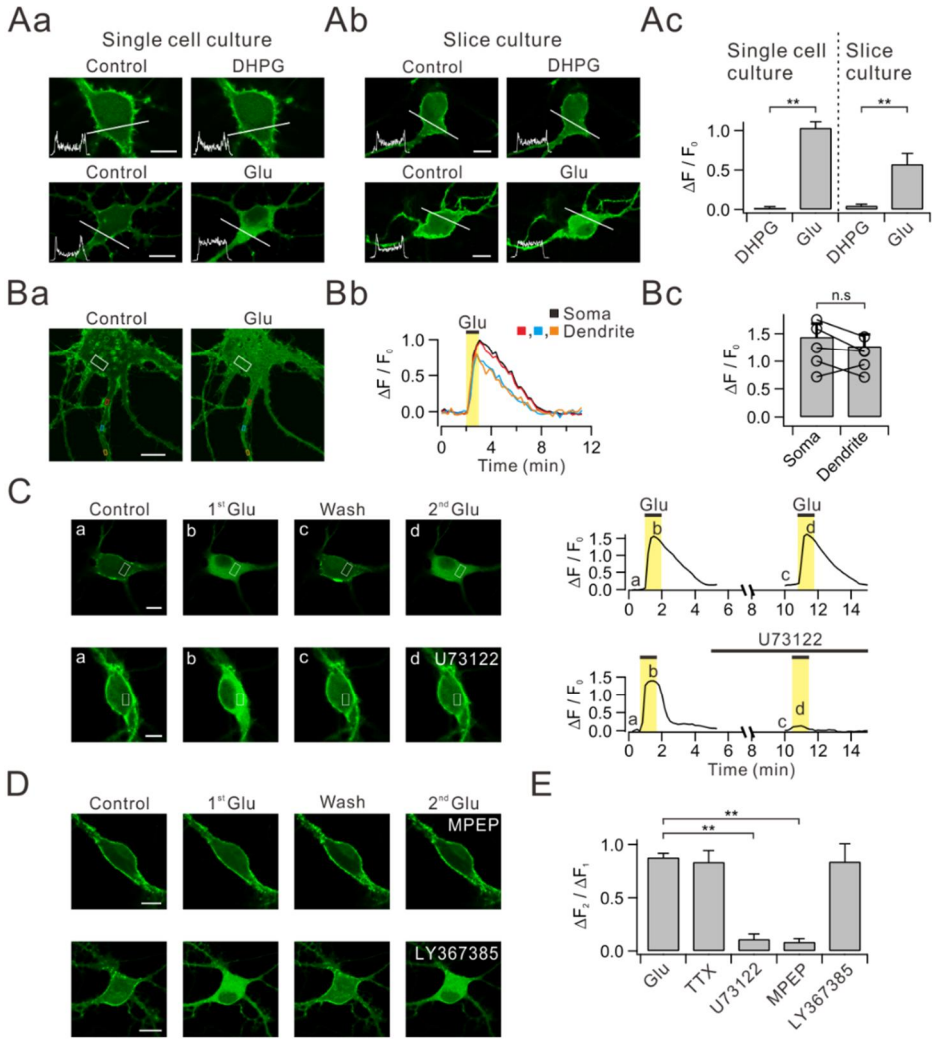

Figure 1. Glutamate, but not DHPG, induces translocation of PHδ-GFP via the mGluR5-PLC pathways. (Aa) Dissociated hippocampal neurons in primary culture (single cell culture) transfected with PHδ-GFP showed prominent green fluorescence signals in plasma membrane versus cytosol ("Control" panels). DHPG ("DHPG" panel) and glutamate ("Glu" panel) was

applied to bath to see if they induce PHδ-GFP translocation. Line profiles of fluorescence intensity (insets) were obtained across the white lines. (Ab) Similar series of experiments were performed with hippocampal neurons in organotypic slice culture transfected with PHδ-GFP. (Ac) Summary data showing the relative amplitudes of DHPG- and glutamate-induced PHδ-GFP translocation ($\Delta F/F_0$) in single cell and slice culture conditions. (Ba) Glutamate-induced PHδ-GFP translocation ($\Delta F/F_0$) was measured in ROIs of somatic cytosol (white) and multiple regions of dendritic cytosol (red, blue and orange). (Bb) Time courses of $\Delta F/F_0$ measured in designated ROIs. (Bc) Bar graphs summarize the amplitudes of DHPG- or glutamate-induced PHδ-GFP translocation in soma and dendrites. (C) Consecutive applications of 30 μM glutamate in control and in the presence of U73122. Images of PHδ-GFP transfected neurons (left panels) and time courses of $\Delta F/F_0$ measured in designated ROIs (right panels). (D) Effect of specific blockers for mGluR5 or mGluR1 on PHδ-GFP translocation. (E) Bar graphs summarize $\Delta F_2/\Delta F_1$ in the presence of TTX and other experimental conditions described in (C) and (D). n.s $p > 0.05$; ** $p < 0.01$. Scale bar = 10 μm in all panels where indicated. Error bars represent SEM.

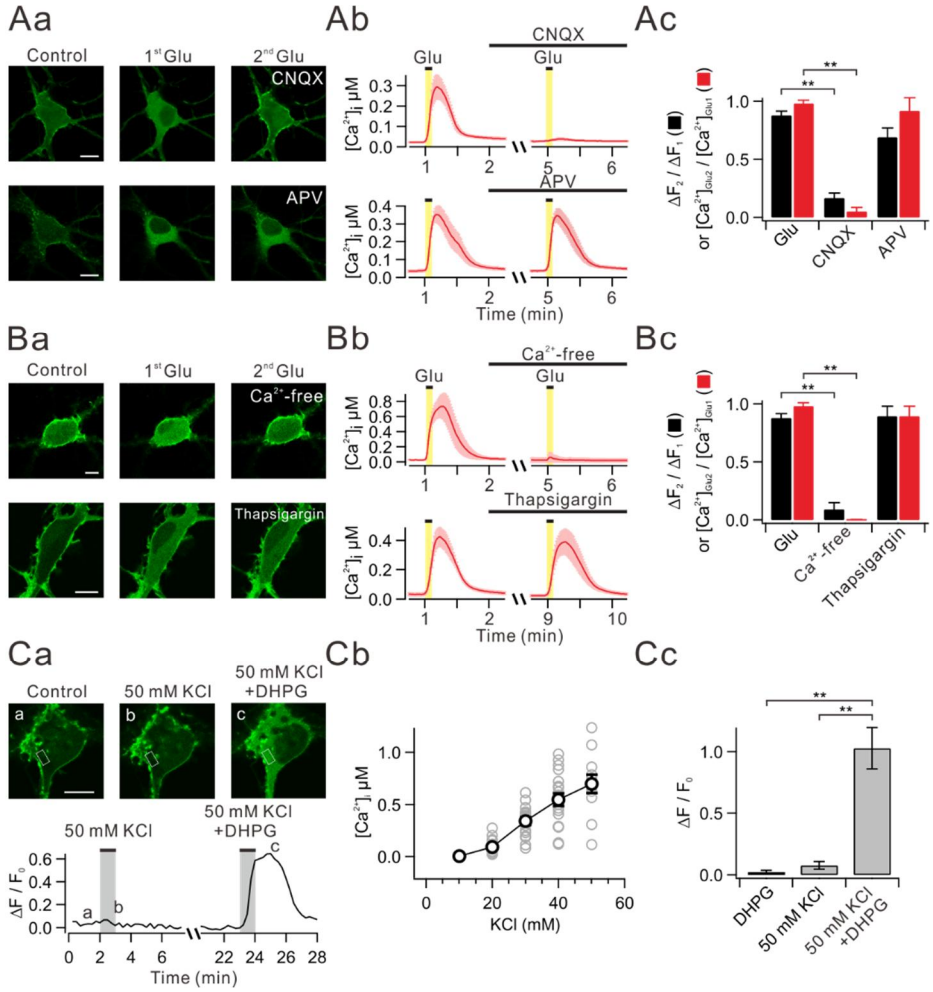

Figure 2. Ca^{2+} influx triggered by AMPA receptor activation facilitates glutamate-induced PHδ-GFP translocation. (Aa) Images demonstrate glutamate-induced translocation of PHδ-GFP in the presence of CNQX (AMPA receptor blocker) and APV (NMDA receptor blocker). (Ab) Glutamate-induced $[Ca^{2+}]_i$ in the presence of CNQX and APV. Error bars are

shown in light colors. (Ac) Bar graphs summarize mean $\Delta F_2/\Delta F_1$ (black) and $[Ca^{2+}]_{Glu2}/[Ca^{2+}]_{Glu1}$ (red). (Ba) Images demonstrate glutamate-induced translocation of PHδ-GFP in Ca^{2+} free solutions or in the presence of thapsigargin (a SERCA blocker). (Bb) Glutamate-induced $[Ca^{2+}]_i$ in experimental conditions described in (Ba). (Bc) Bar graphs summarize mean $\Delta F_2/\Delta F_1$ (black) and $[Ca^{2+}]_{Glu2}/[Ca^{2+}]_{Glu1}$ (red). (Ca) Images of PHδ-GFP translocation induced by 50 mM KCl only or 50 mM KCl plus DHPG (upper panels) and time courses of $\Delta F/F_0$ measured in designated ROIs (lower panel). (Cb) Plot of $[Ca^{2+}]_i$ versus different concentrations of KCl. Gray circles represent individual data. (Cc) $\Delta F/F_0$ values are summarized in bar graph in experimental conditions described in (Ca).** $p < 0.01$. Scale bar = 10 μm in all panels where indicated. Error bars represent SEM.

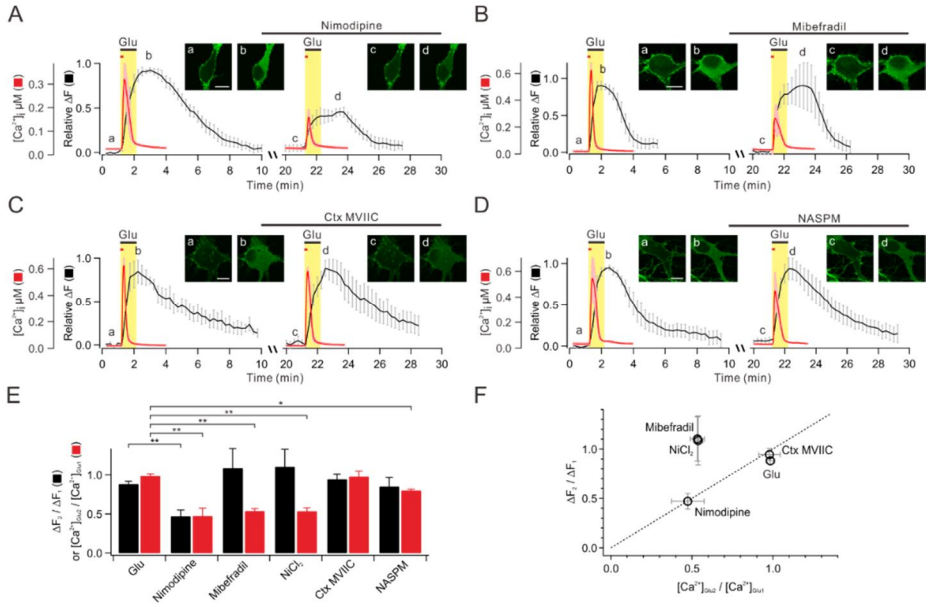

Figure 3. L-type Ca^{2+} channels provide Ca^{2+} for glutamate-induced PHδ-GFP translocation. (A-D) Averages of glutamate-induced $[Ca^{2+}]_i$ (red) and relative ΔF (black) are plotted against time for two successive applications of glutamate (first applications are glutamate only, and second applications are glutamate plus L-, T-, N/P/Q-type Ca^{2+} channel blockers, or Ca^{2+}-permeable AMPA receptor blocker). The time intervals of first and second glutamate applications are actual values (20 min) for ΔF, but for $[Ca^{2+}]_i$ measurements the time intervals were 4 min, as described in Fig. 2Ab: they were superimposed for comparison of time dependent event. The insets show representative images of PHδ-GFP translocation at indicated time points (a-d). Scale bar = 10 μm. (E) Bar graphs summarize mean $\Delta F_2/\Delta F_1$ (black) and

$[Ca^{2+}]_{Glu2}/[Ca^{2+}]_{Glu1}$ (red). (F) $\Delta F_2/\Delta F_1$ values are plotted versus $[Ca^{2+}]_{Glu2}/[Ca^{2+}]_{Glu1}$ values. Dashed line indicates linear relationship. ** $p < 0.01$; * $p < 0.05$. Error bars represent SEM.

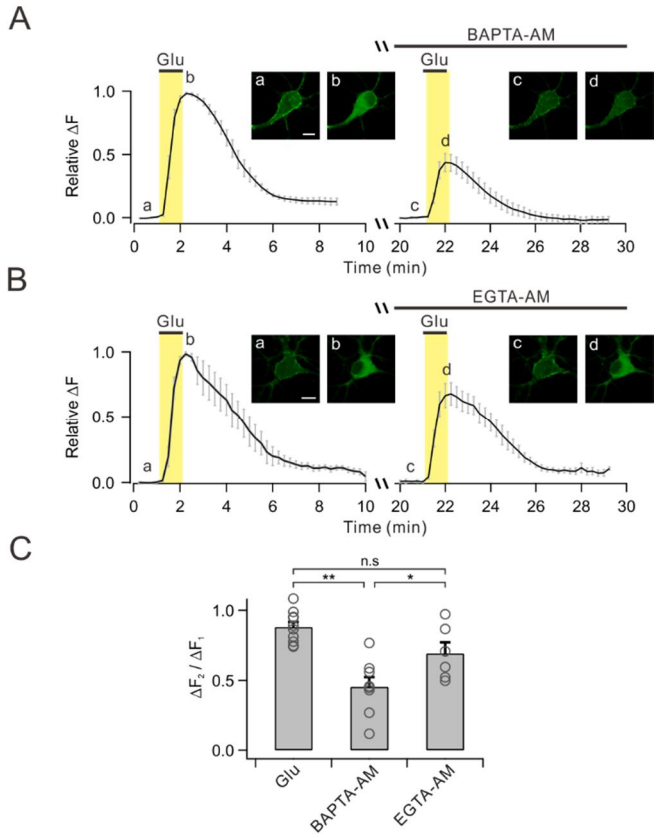

Figure 4. BAPTA, but not EGTA, inhibits glutamate-induced PHδ-GFP translocation. (A-B) Averages of glutamate-induced $\Delta F/F_0$ are plotted against time with BAPTA-AM (A) or EGTA-AM (B) loadings prior to second glutamate applications. The insets show representative images of PHδ-GFP translocation at indicated time points (a-d). Scale bar = 10 μm. (C) Bar graphs summarize mean $\Delta F_2/\Delta F_1$ in experimental conditions described in

(A) and (B). n.s $p > 0.05$; ** $p < 0.01$; * $p < 0.05$. Error bars represent SEM.

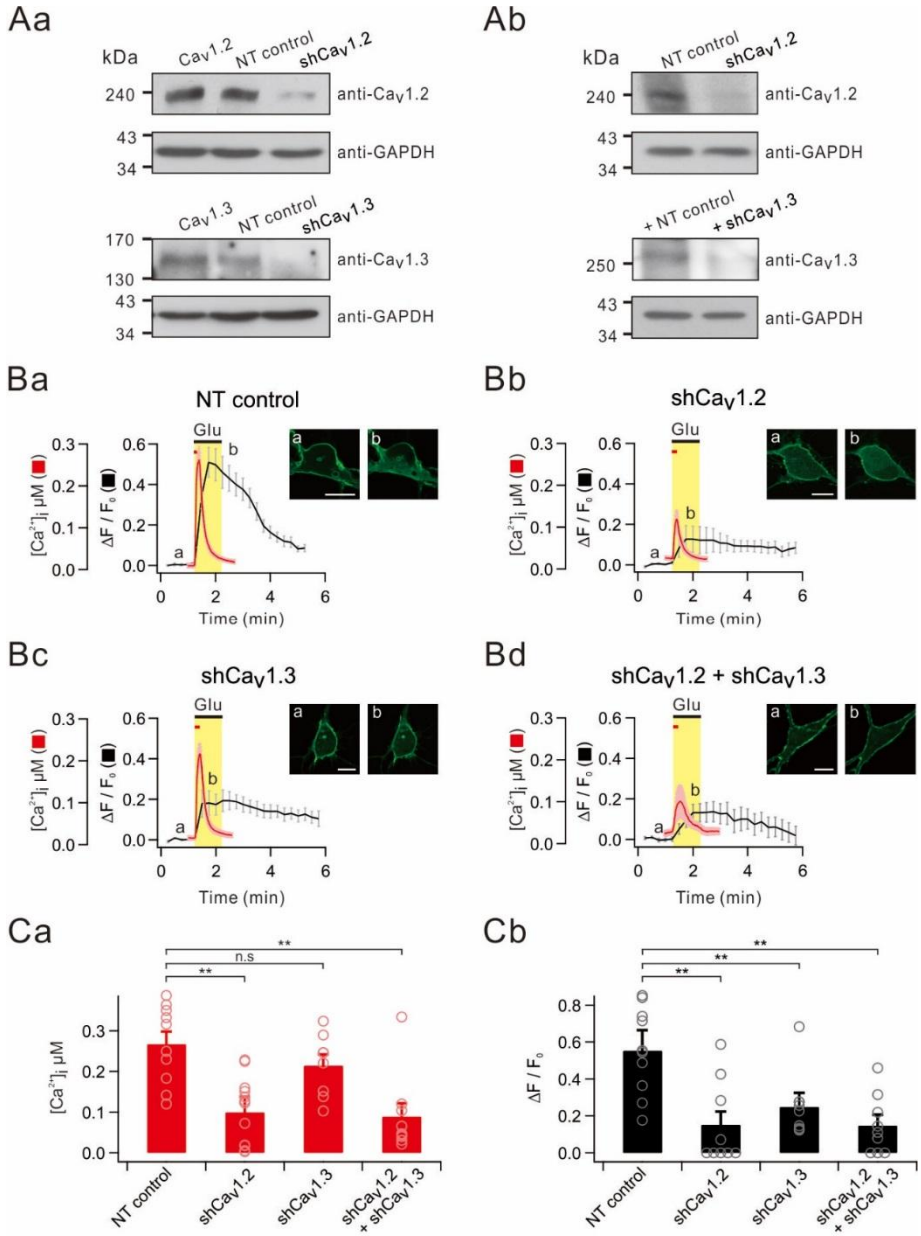

Figure 5. Both $Ca_v1.2$ and $Ca_v1.3$ contribute to glutamate-induced PHδ-GFP translocation. (Aa) Western blotting of over-expressed $Ca_v1.2$ or

$Ca_v1.3$ in HEK 293 cells transfected alone or with non-targeting control (NT control), $Ca_v1.2$ shRNA ($shCa_v1.2$) or $Ca_v1.3$ shRNA ($shCa_v1.3$). (Ab) Western blotting of primary cultured hippocampal neurons transfected with NT control, $shCa_v1.2$ or $shCa_v1.3$. GAPDH served as a loading control. (Ba-Bd) Average of glutamate-induced $[Ca^{2+}]_i$ and $\Delta F/F_0$ are plotted against time in cells transfected with either NT control, $shCa_v1.2$, $shCa_v1.3$ alone or $shCa_v1.2$ and $shCa_v1.3$ together. The insets show representative images of PHδ-GFP translocation at indicated time points (a and b). Scale bar = 10 μm. (C) Bar graph summarizes $[Ca^{2+}]_i$ (Ca) or $\Delta F/F_0$ (Cb) for each group. n.s $p > 0.05$; ** $p < 0.01$. Error bars represent SEM.

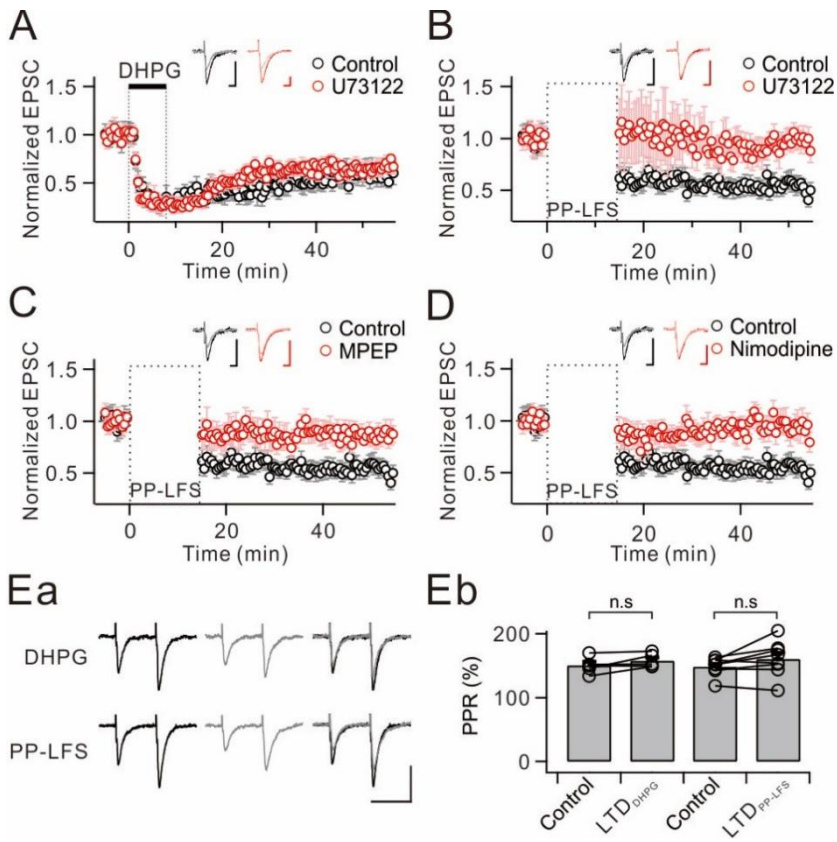

Figure 6. PLC is involved in mGluR-LTD induced by paired-pulse low frequency synaptic stimulation (LTD_{PP-LFS}), but not in mGluR-LTD induced by DHPG (LTD_{DHPG}). EPSC amplitudes were normalized to the pre-DHPG or PP-LFS baseline values and were averaged. (A) DHPG application induced a persistent depression of EPSC amplitude (black). Pre-incubation of slices in U73122 did not affect the magnitude of LTD_{DHPG} (red).

The inset shows representative EPSCs during the baseline period (dark) and 40 min after (light) DHPG application in each condition. (B) PP-LFS induced a similar magnitude of LTD compared to LTD_{DHPG} (black). $LTD_{PP\text{-}LFS}$ was significantly blocked by U73122 (red). (C) Pharmacological blockade of mGluR5 by MPEP almost completely blocked $LTD_{PP\text{-}LFS}$ (red). (D) $LTD_{PP\text{-}LFS}$ was blocked by nimodipine (red). Insets (B-D) represent EPSCs during the baseline period (dark) and 35 min after (light) PP-LFS in each condition. (Ea) Representative EPSCs elicited by paired-pulse stimulation (50 ms interval) during baseline (black, left panels) and after DHPG application or PP-LFS (gray, middle panels). Superimposed traces are shown in right panels. Scale bar = 50 msec (horizontal) and 100 pA (vertical). (Eb) Bar graphs summarize PPR changes in each group. n.s $p > 0.05$. Error bars represent SEM.

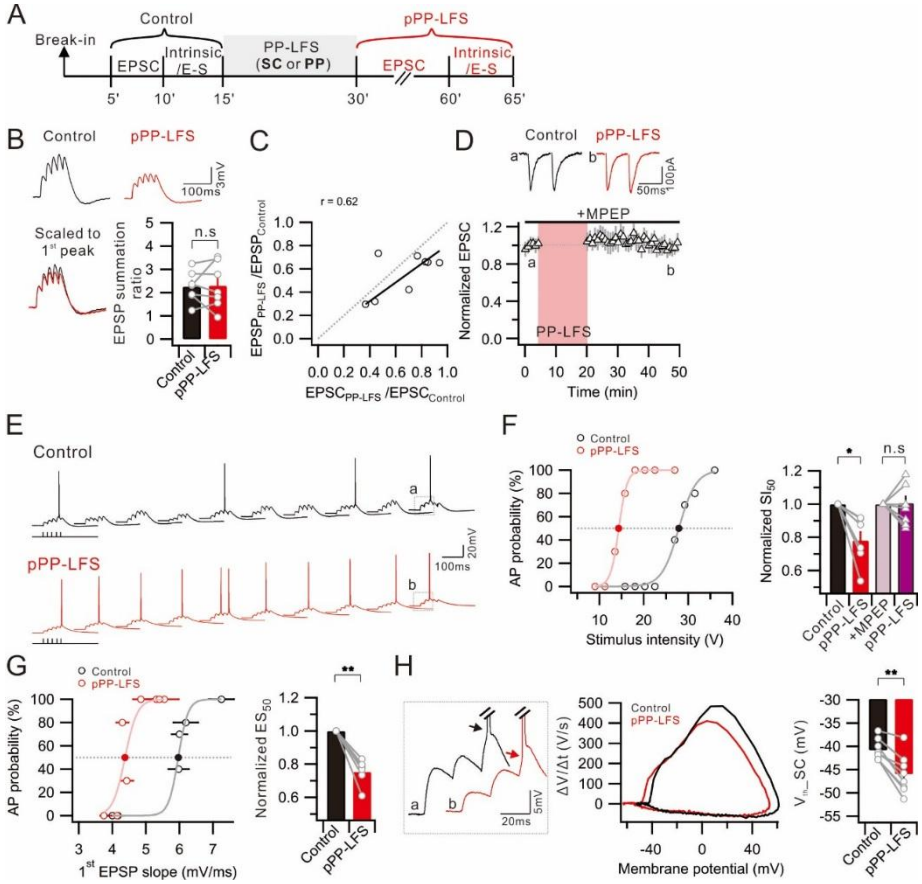

Figure 7. Induction of E-S potentiation during e-LTD$_{PP-LFS}$ at SC-CA1 synapses. (A) Graph illustrating the timeline for the experiment. EPSC recordings at voltage clamping mode and intrinsic parameters and E-S couling recordings at current clampling mode were done before PP-LFS induction (Control) and 30min after PP-LFS (pPP-LFS). (B) Example traces of summated EPSPs by 50Hz SC stimulation are shown on the top. Traces

scaled to 1st EPSP peak are superimposed and shown on the bottom. Bar graphs summarizes no significant change in EPSP summation ratio by PP-LFS. (C) Ratio of first EPSC change ($EPSC_{PP\text{-}LFS}/EPSC_{Control}$) is plotted against EPSP change ($EPSP_{PP\text{-}LFS}/EPSP_{Control}$). Fitted line of data is presented with solid line (black) and a linear correlation is observed ($r = 0.62$). Gray dashed line indicates linear relationship between EPSP and EPSC changes. (D) Presence of MPEP throughout the experiment prevented the induction of $eLTD_{PP\text{-}LFS}$. (E) Raw voltage traces as a result of ten trials of SC stimulation (27 V, 5 stimuli, 50 Hz, 2s interval) before (Control) and 30 min after PP-LFS (pPP-LFS) are shown. After PP-LFS induction, the summated EPSP triggered firing in all trials. (F) Graph showing distribution of firing probability as a function of stimulus voltage before (Control) and 30 min after PP-LFS (pPP-LFS). Firing probability was obtained from 10 trials at each stimulus intensity. Bar graphs show SI_{50} is significantly decreased after PP-LFS, but no significant change occurred in the presence of MPEP. (G) Plot of firing probability as a function of first EPSP slope before (Control)

and 30 min after PP-LFS (pPP-LFS) is shown. Summary data showing significant decrease of ES_{50} after PP-LFS. Sigmoid fitted lines from (F) and (G) are shown with light colors. Filled circles from (F) and (G) indicate where the SI_{50} and the ES_{50} are acquired, respectively. (H) Left, indicated traces marked with (a) and (b) shown at (E) are superimposed and enlarged, showing hyperpolarized V_{th} of APs after PP-LFS. Middle, phase-plane plots of dV/dt versus membrane potential of first AP induced by SC stimulation are shown. Right, bar graphs showing significant V_{th} hyperpolarization that AP induced by SC stimulation (V_{th}_SC). *, $p < 0.05$, **, $p < 0.01$, n.s., $p > 0.05$. Error bars indicate SEM.

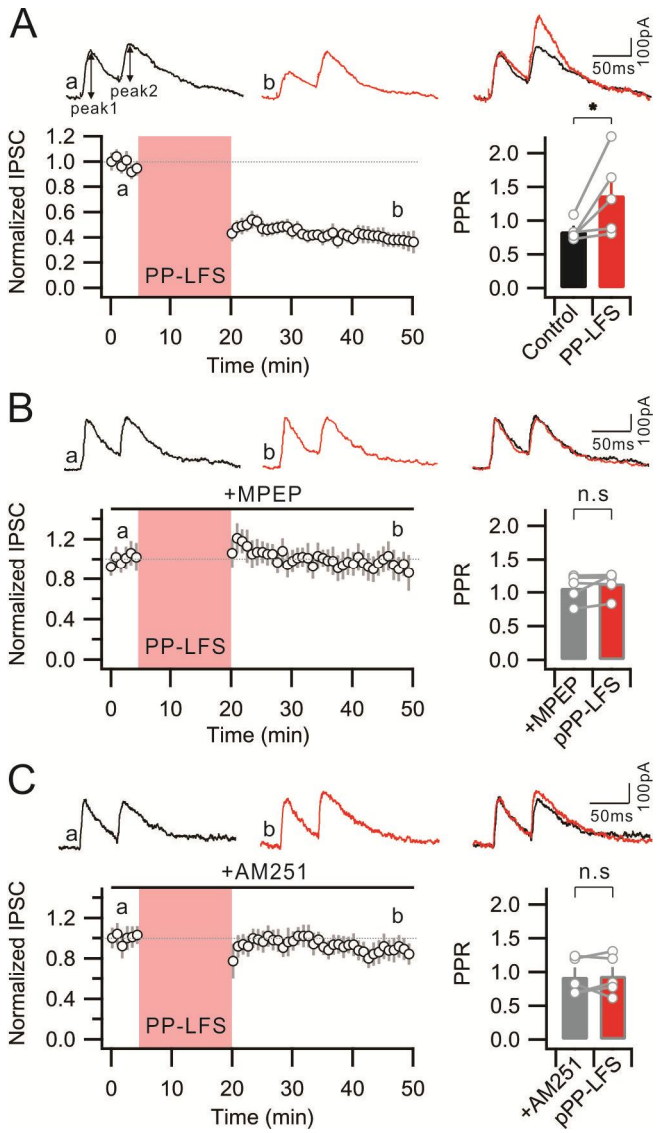

Figure 8. PP-LFS-induced i-LTD is mediated by mGluR/eCB signaling.

(A) Graph showing PP-LFS at SC fibers induced LTD of IPSC magnitude.

Bar graphs showing PPR of IPSC is significantly increased after PP-LFS. (B)

PP-LFS-induced i-LTD is not expressed in the presence of MPEP. The PPR of IPSC is not increased after PP-LFS. (C) Graph showing that the PP-LFS-induced i-LTD is significantly blocked by inhibiting CB_1Rs. The PPR of IPSC in the presence of AM251 remains unchanged after PP-LFS. Insets from (A) to (C), representative IPSC traces before PP-LFS (a, black) and 25–30 min after PP-LFS (b, red) are shown on the top. *, $p < 0.05$, n.s., $p > 0.05$. Error bars indicate SEM.

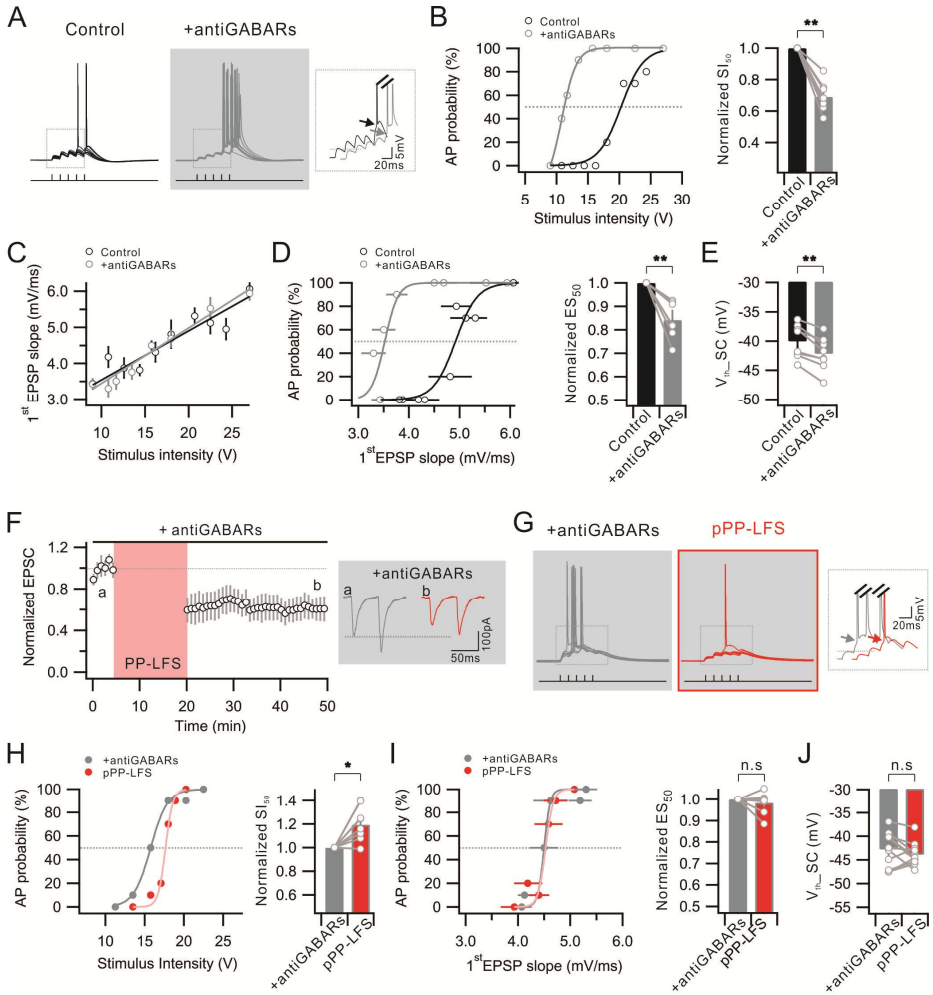

Figure 9. GABA receptor blockers mimic and occlude E-S potentiation associated with V_{th} hyperpolarization during e-LTD$_{PP-LFS}$. (A) Example traces of the voltage responses to 10 trials of suprathreshold SC stimulation obtained before (Control) and after GABARs antagonists application (+antiGABARs) are shown. Inset shows superimposed voltage traces

indicating hyperpolarized V_{th}. (B) Graph showing distribution of firing probability as a function of stimulus voltage before (Control) and after antiGABARs application (+antiGABARs). Bar graph summarizes significant decrease of SI_{50} by GABARs blockade. (C) No significant change is detected in the ratio of the first EPSP slope to stimulus intensity after the antiGABARs application. (D) Plot of firing probability as a function of first EPSP slope is shown. Bar graphs summarize a significant decrease in ES_{50} by GABARs inhibition. (E) Summary data showing significant V_{th} hyperpolarization that APs induced by SC stimulation (V_{th}_SC). (F) The e-$LTD_{PP\text{-}LFS}$ is still induced in the presence of antiGABARs. Inset, EPSC traces obtained before (a) and 25–30 min after PP-LFS (b) are shown. (G) Voltage responses to 10 trials of suprathreshold SC stimulation before (+antiGABARs) and after PP-LFS (pPP-LFS) in the presence of antiGABARs during entire recordings are shown. Inset indicating no significant change in V_{th}. (H) Distribution of firing probability as a function of stimulus voltage before (+antiGABARs) and after PP-LFS (pPP-LFS) in

the presence antiGABARs is shown. Right, bar graphs summarize significant increase in SI_{50}. (I) No significant change is detected in AP probability versus 1st EPSP slope. Bar graphs summarize no significant change in ES_{50}. (J) V_{th} shift by PP-LFS is occluded in the presence of antiGABARs. *, $p < 0.05$, **, $p < 0.01$, n.s., $p > 0.05$. Error bars indicate SEM.

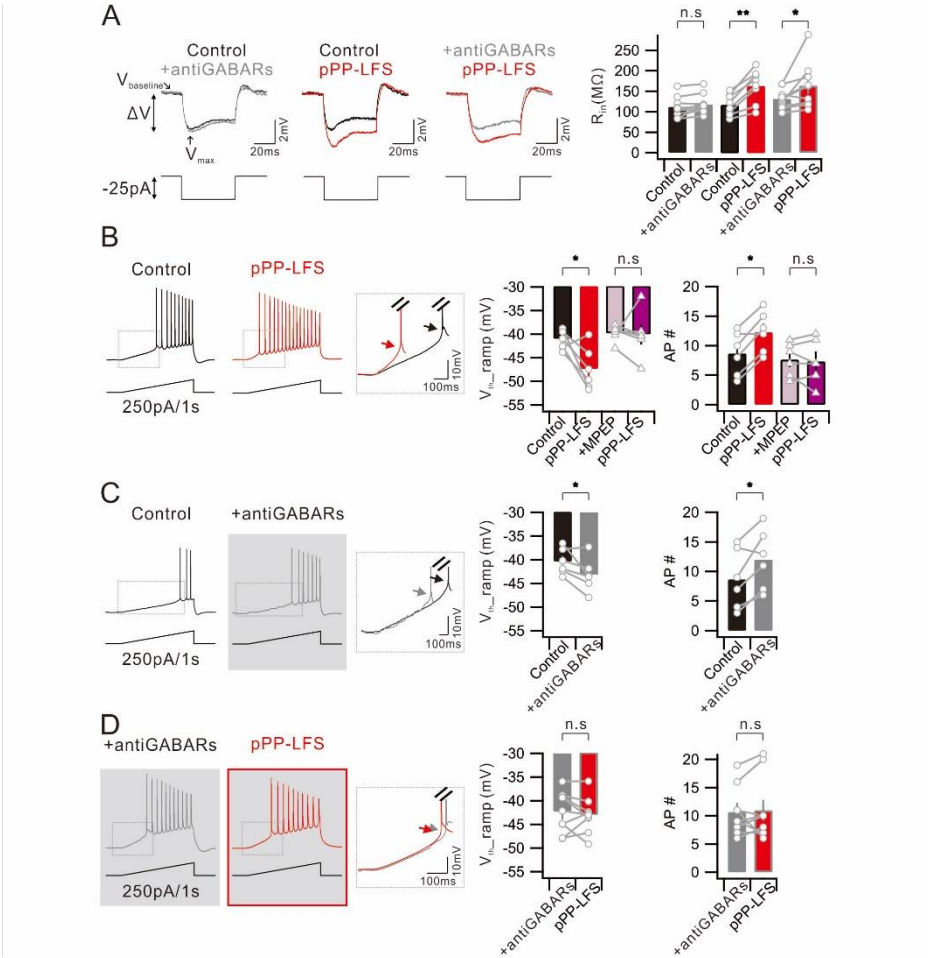

Figure 10. V_{th} hyperpolarization for APs evoked by somatic depolarization during e-LTD_{PP-LFS} is dependent on GABAergic mechanisms. (A) Left, representative traces showing the voltage responses to a -25pA square current injection. Traces obtained in condition before (Control) and after antiGABARs application (+antiGABARs); before

(Control) and 30min after PP-LFS (pPP-LFS); before (+antiGABARs) and after PP-LFS (pPP-LFS) in the presence of antiGABARs during the entire recordings are superimposed ($V_{baseline}$: baseline of voltage deflection; $V_{baseline}$: maximum point of voltage deflection). Right, summary bar graphs of the R_{in} profile obtained under described conditions. (B) Representative voltage responses to a ramp (250 pA/1 s) current injection to soma before (Control) and 30 min after PP-LFS (pPP-LFS) are shown. Inset shows superimposed traces of significant V_{th} hyperpolarization of first AP. Bar graphs summarize significant V_{th} hyperpolarization (V_{th}_ramp) and increase in number of AP (AP #). Presence of MPEP throughout the experiment prevented the changes in V_{th} and number of AP. (C) The same ramp protocol is performed before (Control) and after perfusion of antiGABARs (+antiGABARs). (D) The same ramp protocol is performed in the presence of antiGABARs (+antiGABARs) and compared with the subsequent PP-LFS induction (pPP-LFS). *, $p < 0.05$, **, $p < 0.01$, n.s., $p > 0.05$. Error bars indicate SEM.

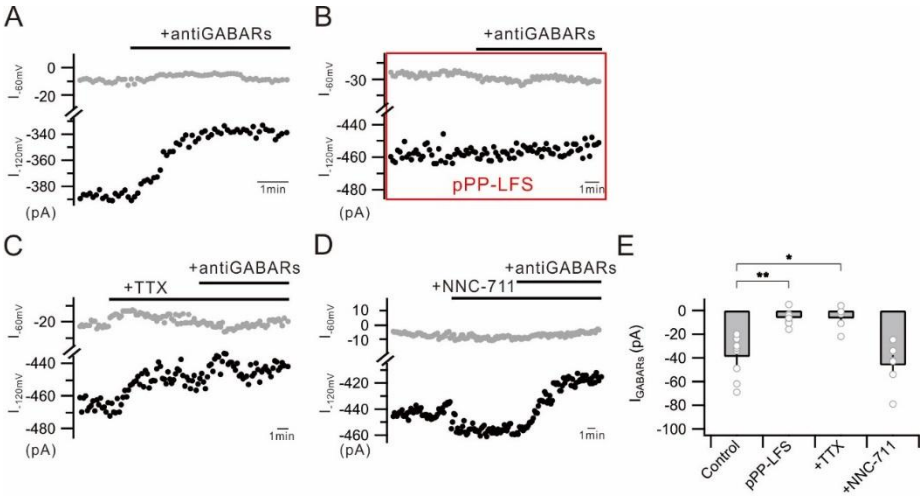

Figure 11. PP-LFS inhibits tonic GABA currents. (A) Graph showing recorded currents at −60 mV (I_{-60mV}, gray) or −120 mV (I_{-120mV}, black) holding. Consistent reduction of currents by antiGABARs perfusion (+antiGABARs) is well detected at −120 mV holding. (B) I_{GABARs} was no longer detected after pPP-LFS induction (pPP-LFS). (C) I_{-120mV} is reduced by TTX perfusion (+TTX) and is not further reduced by subsequent antiGABARs treatment (+antiGABARs). (D) I_{-120mV} is slightly increased by NNC-711 perfusion (+NNC-711) and reduced by subsequent antiGABARs treatment (+antiGABARs). (E) Bar graphs summarize I_{GABARs} in conditions described from (A) to (D). *, $p < 0.05$, **, $p < 0.01$. Error bars indicate SEM.

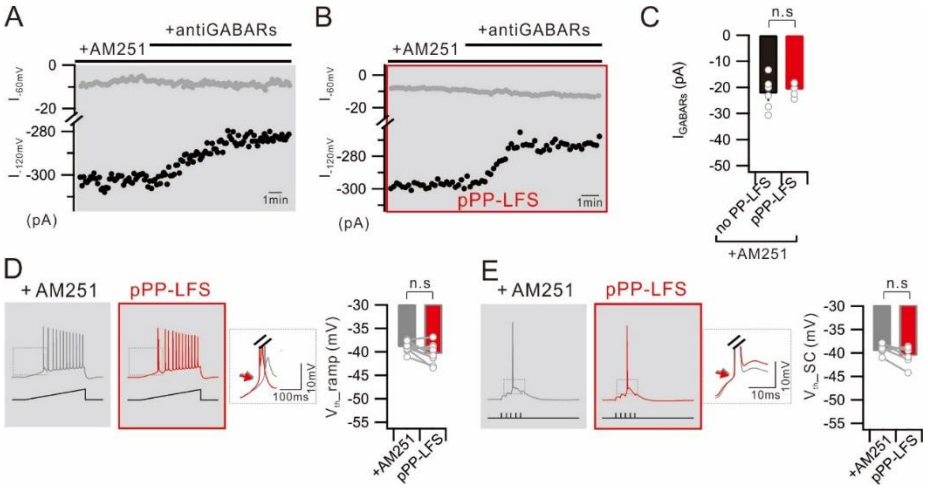

Figure 12. PP-LFS-induced reduction of tonic inhibition is mediated by eCB/CB$_1$R activation. (A) Graph showing that I_{GABARs} is detected at −120 mV holding in the presence of AM251 (+AM251) during entire recordings. (B) In the presence of AM251 (+AM251), I_{GABARs} is still detected at −120 mV holding after PP-LFS (pPP-LFS). (C) Bar graph summarizes measured I_{GABARs} without PP-LFS (no PP-LFS) or after PP-LFS induction (pPP-LFS) in the presence of AM251. (D) Ramp current induced voltage traces with CB_1Rs blocking (+AM251) and 30 min after PP-LFS (pPP-LFS) are shown. Summarized data showing no significant change in V_{th}_ramp. (E) Suprathreshold SC stimulation induced voltage traces before (+AM251) and

30 min after PP-LFS (pPP-LFS) with AM251 perfusion. Bar graphs showing no significant change in V_{th}_SC. Insets, superimposed and expanded traces from the boxed area are shown. Arrows indicate no significant change of V_{th}. n.s, $p > 0.05$. Error bars indicate SEM.

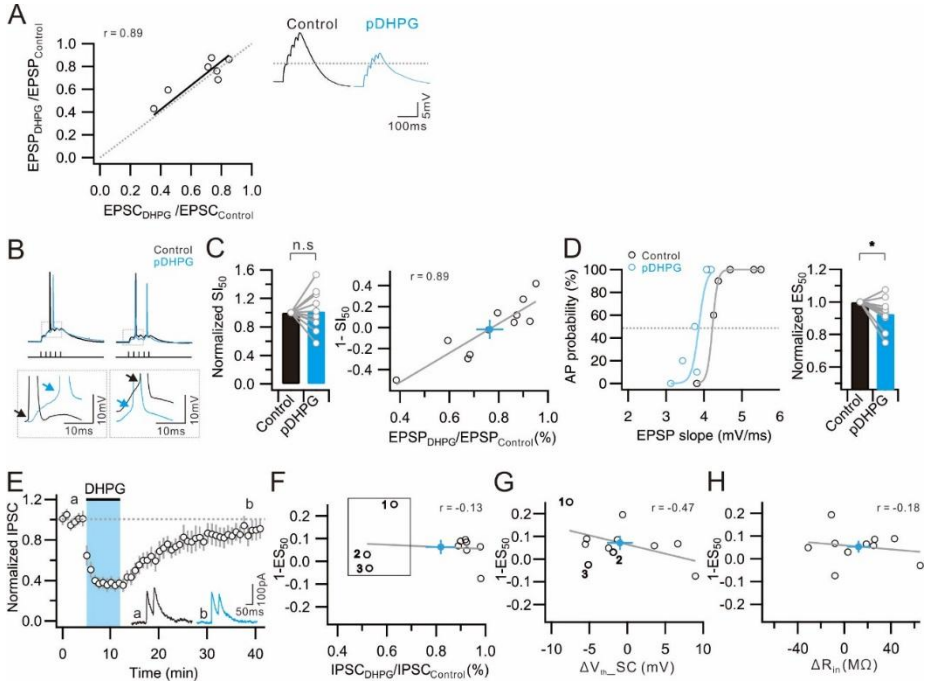

Figure 13. DHPG induce e-LTD with weak E-S potentiation, but no significant i-LTD. (A) Ratio of first EPSP change ($EPSP_{DHPG}/EPSP_{Control}$) is plotted against first EPSC change ($EPSP_{DHPG}/EPSP_{Control}$). Fitted line of data is presented with solid line (black) and a linear correlation is observed (r = 0.89). Representative traces of EPSPs during the base line period (0–5 min) (Control, black) and 25–30 min after DHPG application (pDHPG, light blue) are shown on the right. (B) Representative voltage traces by suprathreshold SC stimulation before (Control) and after DHPG application (pDHPG) are

shown. Insets show DHPG-induced variable results in depolarization (left) or hyperpolarization (right) of V_{th}. (C) Bar graphs summarize no significant changes in SI_{50}. Graph shows strong linear relationship between 1-SI_{50} and EPSP weight (r = 0.89). (D) Distribution of firing probability as a function of EPSP slope before (Control) and 30 min after DHPG application (pDHPG) is shown. Sigmoid fitted line is shown with light colors. Bar graphs summarize significant decrease in ES_{50}. (E) Time course and magnitude of i-LTD by DHPG application are shown. Inset, representative IPSC traces obtained before (a) and 25–30 min after DHPG application (b) are shown. (F) No correlation is detected between 1-ES_{50} and IPSC weight (r = −0.13). Samples that show IPSC decreases more than 20% after DHPG are numbered and indicated with box. (G) Graph showing a linear correlation between 1-ES_{50} and ΔV_{th}_SC (r = −0.47). Numbers indicate 3 cells that show significant i-LTD in Fig. 7F. (H) No correlation is detected between 1-ES_{50} and ΔR_{in} (r = −0.18). Closed circles (light blue) and gray solid lines at (C), (F), (G), and (H) indicate averaged number and fitted line of data,

respectively. Error bars indicate SEM. *, $p < 0.05$, n.s., $p > 0.05$.

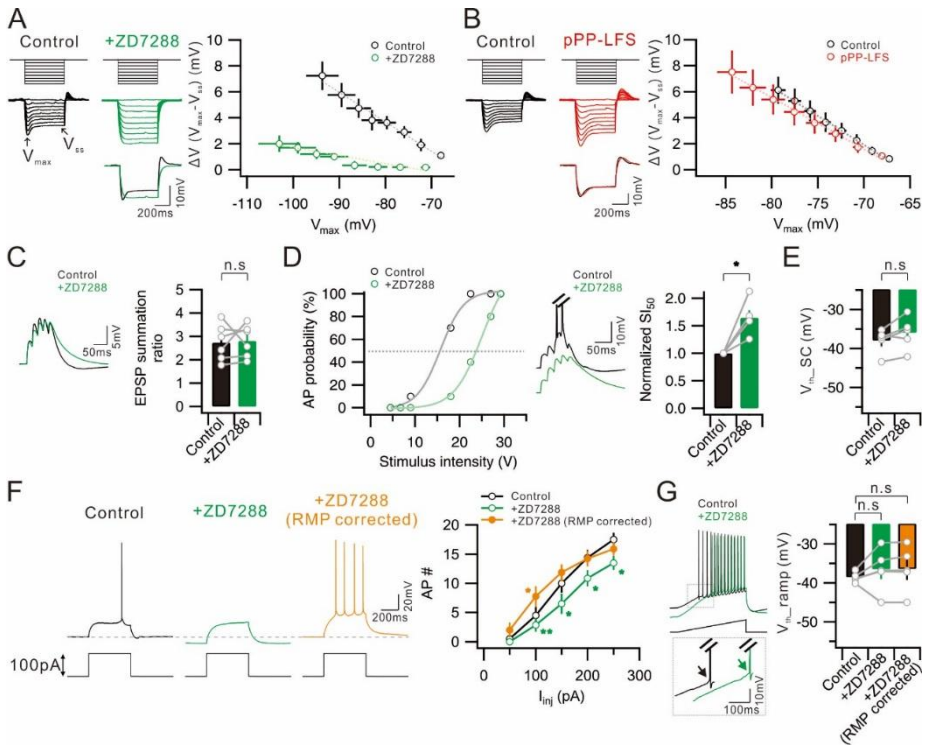

Figure 14. Effects of ZD7288, I_h blocker, on intrinsic excitability and E-S coupling in CA1 neurons. (A) Left, voltage deflections in response to a series of current steps (−200 to 0 pA, 25 pA increment) before (Control) and after ZD7288 application (+ZD7288) are shown (V_{max}: maximum point of voltage deflection; V_{ss}: steady state of voltage deflection). Voltage response to −200 pA current injection in Control and the similar level of V_{max} shown at +ZD7288 are superimposed and shown on the bottom. Right, ΔV (V_{max}-

V_{ss}) is plotted against V_{max} before (Control) and after ZD7288 application (+ZD7288). (B) Left, representative voltage deflections to current steps before (Control) and 30 min after PP-LFS (pPP-LFS) are shown. Right, ΔV (V_{max}-V_{ss}) versus V_{max} in Control and after PP-LFS are plotted with black and red colors, respectively. (C) Left, example traces of EPSP before (Control) and after ZD7288 application (+ZD7288) by subthreshold synaptic stimulation at 50Hz. Bar graphs summarize no significant changes in EPSP summation ratio by ZD7288 application. (D) Left, plot of firing probability as a function of stimulus intensity before (Control) and after ZD7288 application (+ZD7288) is shown. Middle, example traces of voltage changes in response to a same intensity of synaptic stimulation. Note the decrease in AP firing with the I_h inhibition. Right, summary graphs of increased SI_{50} by I_h inhibition. (E) Bar graphs summarize no significant changes in V_{th}_SC in the presence of ZD7288. (F) Left, representative voltage traces to current step (100pA) before (Control), after ZD7288 application (+ZD7288) and RMP corrected with current injection (+ZD7288 (RMP corrected)) are

shown. Right, summary data showing significant decrease in AP firing in the presence of ZD7288. There was an increase in AP firing by correcting RMP. (G) Voltage responses to ramp current injection before (Control) and after ZD7288 application (+ZD7288) are shown. Inset, traces at boxed area are superimposed and shown on the bottom. Bar graphs summarize no significant changes in V_{th}_ramp. (F) *, $p < 0.05$, **, $p < 0.01$, n.s., $p > 0.05$. Error bars indicate SEM.

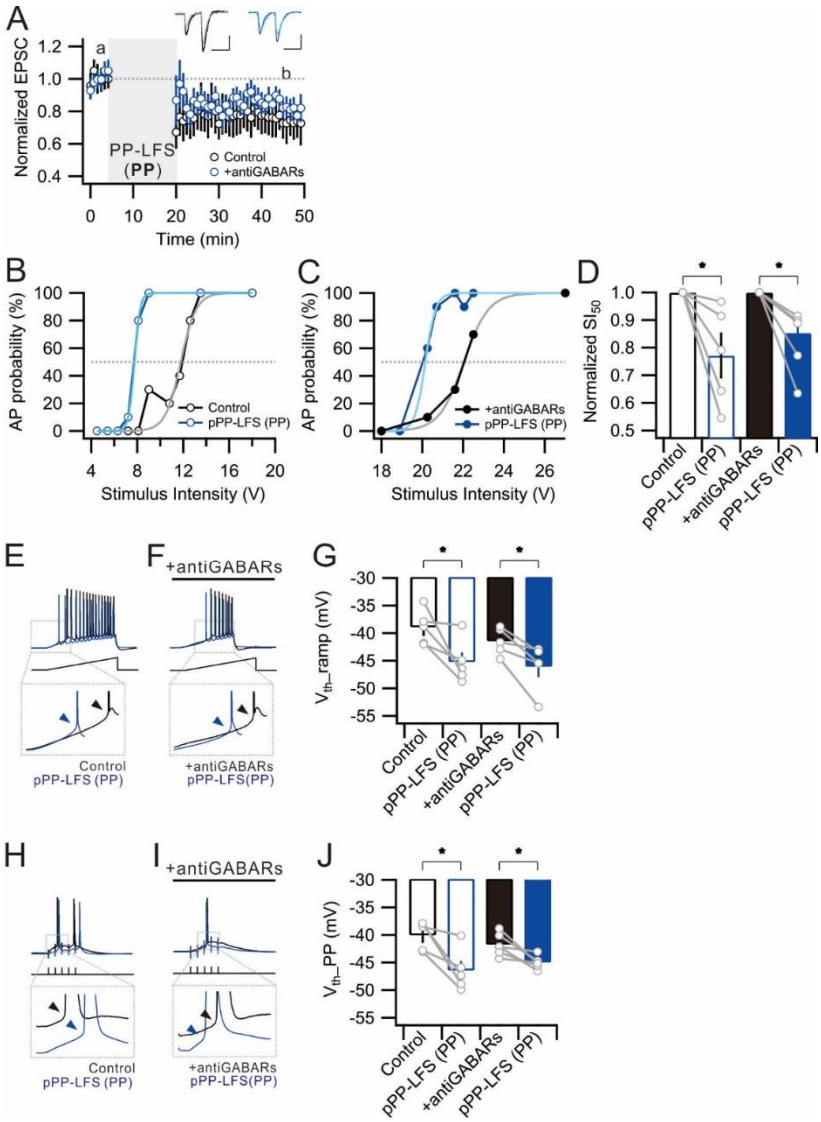

Figure 15. PP-LFS induced change in I-O relationship at perforant pathway-CA1 synapses is independent on inhibitory input. (A) Graph showing PP-LFS at perforant pathway induced long-term change in EPSC

magnitude (Control, black). PP-LFS induced LTD is still expressed while blocking GABARs at perforant pathway-CA1 synapses (+antiGABARs, blue). Representative EPSC traces indicated at (a) and (b) are superimposed in an each conditions. Scale bar = 50 msec (horizontal) and 100 pA (vertical). (B) Graph showing distribution of firing probability as function of stimulus voltage before (Control, black) and 30 min after PP-LFS (pPP-LFS (PP), blue). (C) Graph showing distribution of firing probability as function of stimulus voltage before (+antiGABARs, black) and 30 min after PP-LFS (pPP-LFS (PP), blue) while blocking GABARs. Sigmoid fitted lines are shown as light color. (D) Bar graphs summarize significant change in SI_{50} in an each conditions. (E) Ramp current induced voltage traces before (left, black) and 30 min after PP-LFS induction (right, blue) are superimposed. (F) Ramp current induced voltage traces before (left, black) and 30 min after PP-LFS induction (right, blue) in the presence of GABARs blockers are superimposed. (G) Bar graphs showing significant hyperpolarization of V_{th}_ramp in an each conditions described in (E) and (F). (H) Supra-threshold

perforant pathway stimulation (5 pulses, 50 Hz) induced voltage traces before (left, black) and 30 min after PP-LFS (right, blue) are superimposed. (I) Supra-threshold perforant pathway stimulation (5 pulses, 50 Hz) induced voltage traces before (left, black) and 30 min after PP-LFS (right, blue) are superimposed in the presence of GABARs blockers. (J) Bar graphs showing significant hyperpolarization of V_{th}_PP in an each conditions described in (H) and (I). Insets from (E), (F), (H) and (I), traces at the boxed region are superimposed and expanded. Arrows indicate significant changes of V_{th}. n.s, $p > 0.05$, *, $p < 0.05$. Error bars indicate SEM.

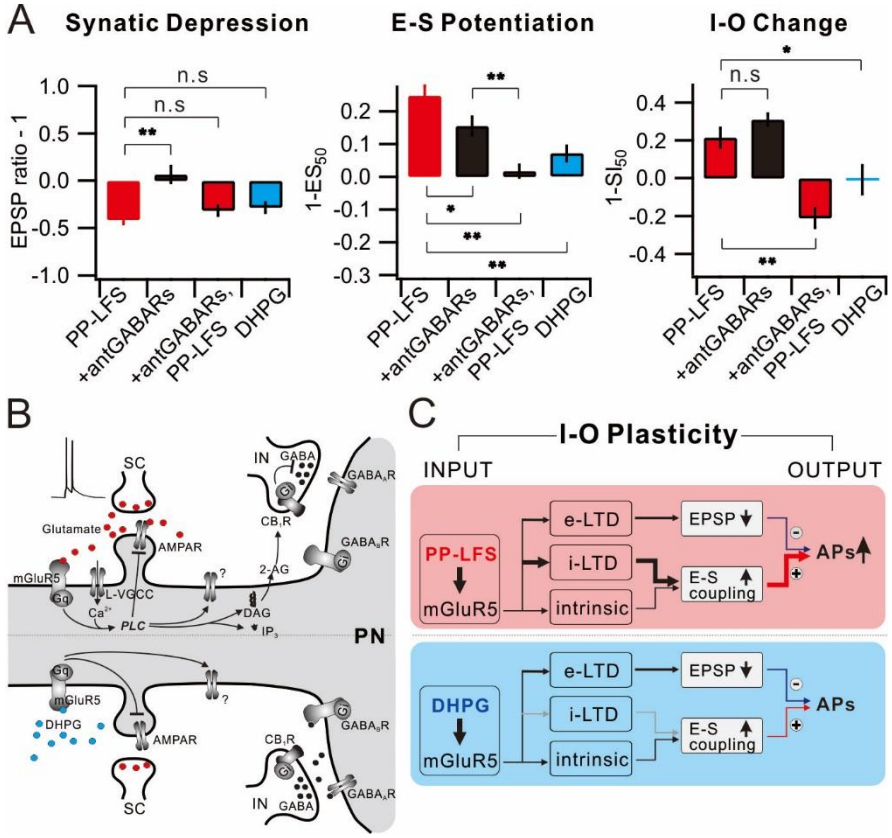

Figure 16. Understanding I–O plasticity during e-LTD by integration of synaptic plasticity and E-S potentiation. (A) Summarized data of changes in synaptic weight (left), E-S coupling (middle), and I–O change (right) in each condition. (B) Illustration of mGluR5-dependent downstream signaling mechanism induced by synaptic stimulation (upper panel) or DHPG application (lower panel) in CA1 pyramidal neuron. Gq, Gq protein; L-

VGCC, L-type voltage gated Ca^{2+} channel; AMPAR, AMPA receptor; IP_3, inositol trisphosphate; IN, interneuron; PN, pyramidal neuron (C) Schematic diagram of I–O plasticity. *, $p < 0.05$, **, $p < 0.01$, n.s., $p > 0.05$. Error bars indicate SEM.

REFERENCES

Abe, T., Sugihara, H., Nawa, H., Shigemoto, R., Mizuno, N., and Nakanishi, S. (1992). Molecular characterization of a novel metabotropic glutamate receptor mGluR5 coupled to inositol phosphate/Ca^{2+} signal transduction. The Journal of biological chemistry *267*, 13361-13368.

Abraham, W.C., Gustafsson, B., and Wigstrom, H. (1987). Long-term potentiation involves enhanced synaptic excitation relative to synaptic inhibition in guinea-pig hippocampus. The Journal of physiology *394*, 367-380.

Aramori, I., and Nakanishi, S. (1992). Signal transduction and pharmacological characteristics of a metabotropic glutamate receptor, mGluR1, in transfected CHO cells. Neuron *8*, 757-765.

Bear, M.F., and Malenka, R.C. (1994). Synaptic plasticity: LTP and LTD. Current opinion in neurobiology *4*, 389-399.

Biel, M., Wahl-Schott, C., Michalakis, S., and Zong, X. (2009). Hyperpolarization-activated cation channels: from genes to function. Physiological reviews *89*, 847-885.

Bliss, T.V., and Collingridge, G.L. (1993). A synaptic model of memory:

long-term potentiation in the hippocampus. Nature *361*, 31-39.

Bolshakov, V.Y., and Siegelbaum, S.A. (1994). Postsynaptic induction and presynaptic expression of hippocampal long-term depression. Science *264*, 1148-1152.

Brager, D.H., and Johnston, D. (2007). Plasticity of intrinsic excitability during long-term depression is mediated through mGluR-dependent changes in I_h in hippocampal CA1 pyramidal neurons. J Neurosci *27*, 13926-13937.

Bright, D.P., and Smart, T.G. (2013). Methods for recording and measuring tonic $GABA_A$ receptor-mediated inhibition. Front Neural Circuits *7*, 193.

Campanac, E., Daoudal, G., Ankri, N., and Debanne, D. (2008). Downregulation of dendritic I_h in CA1 pyramidal neurons after LTP. J Neurosci *28*, 8635-8643.

Castillo, P.E. (2012). Presynaptic LTP and LTD of excitatory and inhibitory synapses. Cold Spring Harb Perspect Biol *4*.

Castillo, P.E., Younts, T.J., Chavez, A.E., and Hashimotodani, Y. (2012). Endocannabinoid signaling and synaptic function. Neuron *76*, 70-81.

Chavez-Noriega, L.E., Bliss, T.V., and Halliwell, J.V. (1989). The EPSP-spike (E-S) component of long-term potentiation in the rat hippocampal slice is modulated by GABAergic but not cholinergic mechanisms. Neurosci Lett

104, 58-64.

Chavez-Noriega, L.E., Halliwell, J.V., and Bliss, T.V. (1990). A decrease in firing threshold observed after induction of the EPSP-spike (E-S) component of long-term potentiation in rat hippocampal slices. Exp Brain Res *79*, 633-641.

Chevaleyre, V., and Castillo, P.E. (2003). Heterosynaptic LTD of hippocampal GABAergic synapses: a novel role of endocannabinoids in regulating excitability. Neuron *38*, 461-472.

Chevaleyre, V., and Castillo, P.E. (2004). Endocannabinoid-mediated metaplasticity in the hippocampus. Neuron *43*, 871-881.

Conn, P.J., and Pin, J.P. (1997). Pharmacology and functions of metabotropic glutamate receptors. Annual review of pharmacology and toxicology *37*, 205-237.

Connelly, W.M., Fyson, S.J., Errington, A.C., McCafferty, C.P., Cope, D.W., Di Giovanni, G., and Crunelli, V. (2013). $GABA_B$ Receptors Regulate Extrasynaptic $GABA_A$ Receptors. J Neurosci *33*, 3780-3785.

Dalby, N.O. (2003). Inhibition of gamma-aminobutyric acid uptake: anatomy, physiology and effects against epileptic seizures. Eur J Pharmacol *479*, 127-137.

De Simoni, A., and Yu, L.M. (2006). Preparation of organotypic hippocampal slice cultures: interface method. Nature protocols *1*, 1439-1445.

Doherty, A.J., Palmer, M.J., Henley, J.M., Collingridge, G.L., and Jane, D.E. (1997). (RS)-2-chloro-5-hydroxyphenylglycine (CHPG) activates mGlu5, but no mGlu1, receptors expressed in CHO cells and potentiates NMDA responses in the hippocampus. Neuropharmacology *36*, 265-267.

Edwards, D.A., Zhang, L., and Alger, B.E. (2008). Metaplastic control of the endocannabinoid system at inhibitory synapses in hippocampus. Proceedings of the National Academy of Sciences of the United States of America *105*, 8142-8147.

Eggermann, E., and Jonas, P. (2012). How the 'slow' Ca^{2+} buffer parvalbumin affects transmitter release in nanodomain-coupling regimes. Nat Neurosci *15*, 20-22.

El-Hassar, L., Hagenston, A.M., D'Angelo, L.B., and Yeckel, M.F. (2011). Metabotropic glutamate receptors regulate hippocampal CA1 pyramidal neuron excitability via Ca^{2+} wave-dependent activation of SK and TRPC channels. The Journal of physiology *589*, 3211-3229.

Fitzjohn, S.M., Palmer, M.J., May, J.E., Neeson, A., Morris, S.A., and Collingridge, G.L. (2001). A characterisation of long-term depression

induced by metabotropic glutamate receptor activation in the rat hippocampus in vitro. The Journal of physiology *537*, 421-430.

Gamper, N., Reznikov, V., Yamada, Y., Yang, J., and Shapiro, M.S. (2004). Phosphatidylinositol 4,5-bisphosphate signals underlie receptor-specific $G_{q/11}$-mediated modulation of N-type Ca^{2+} channels. J Neurosci *24*, 10980-10992.

Gasselin, C., Inglebert, Y., Ankri, N., and Debanne, D. (2017). Plasticity of intrinsic excitability during LTD is mediated by bidirectional changes in h-channel activity. Sci Rep *7*, 14418.

Glykys, J., and Mody, I. (2006). Hippocampal network hyperactivity after selective reduction of tonic inhibition in $GABA_A$ receptor alpha5 subunit-deficient mice. Journal of neurophysiology *95*, 2796-2807.

Glykys, J., and Mody, I. (2007). The main source of ambient GABA responsible for tonic inhibition in the mouse hippocampus. The Journal of physiology *582*, 1163-1178.

Hashimotodani, Y., Ohno-Shosaku, T., Tsubokawa, H., Ogata, H., Emoto, K., Maejima, T., Araishi, K., Shin, H.S., and Kano, M. (2005). Phospholipase Cbeta serves as a coincidence detector through its Ca^{2+} dependency for triggering retrograde endocannabinoid signal. Neuron *45*, 257-268.

Heifets, B.D., and Castillo, P.E. (2009). Endocannabinoid signaling and long-term synaptic plasticity. Annu Rev Physiol *71*, 283-306.

Hell, J.W., Westenbroek, R.E., Warner, C., Ahlijanian, M.K., Prystay, W., Gilbert, M.M., Snutch, T.P., and Catterall, W.A. (1993). Identification and differential subcellular localization of the neuronal class C and class D L-type calcium channel alpha 1 subunits. The Journal of cell biology *123*, 949-962.

Holbro, N., Grunditz, A., and Oertner, T.G. (2009). Differential distribution of endoplasmic reticulum controls metabotropic signaling and plasticity at hippocampal synapses. Proc Natl Acad Sci U S A *106*, 15055-15060.

Horowitz, L.F., Hirdes, W., Suh, B.C., Hilgemann, D.W., Mackie, K., and Hille, B. (2005). Phospholipase C in living cells: activation, inhibition, Ca^{2+} requirement, and regulation of M current. The Journal of general physiology *126*, 243-262.

Ireland, D.R., and Abraham, W.C. (2002). Group I mGluRs increase excitability of hippocampal CA1 pyramidal neurons by a PLC-independent mechanism. J Neurophysiol *88*, 107-116.

Kaech, S., and Banker, G. (2006). Culturing hippocampal neurons. Nat. Protocols *1*, 2406-2415.

Kano, M., Hashimoto, K., and Tabata, T. (2008). Type-1 metabotropic glutamate receptor in cerebellar Purkinje cells: a key molecule responsible for long-term depression, endocannabinoid signalling and synapse elimination. Philosophical transactions of the Royal Society of London. Series B, Biological sciences *363*, 2173-2186.

Kato, H.K., Kassai, H., Watabe, A.M., Aiba, A., and Manabe, T. (2012). Functional coupling of the metabotropic glutamate receptor, InsP3 receptor and L-type Ca^{2+} channel in mouse CA1 pyramidal cells. The Journal of physiology *590*, 3019-3034.

Kim, H.H., Lee, K.H., Lee, D., Han, Y.E., Lee, S.H., Sohn, J.W., and Ho, W.K. (2015). Costimulation of AMPA and metabotropic glutamate receptors underlies phospholipase C activation by glutamate in hippocampus. J Neurosci *35*, 6401-6412.

Kim, J., Dittgen, T., Nimmerjahn, A., Waters, J., Pawlak, V., Helmchen, F., Schlesinger, S., Seeburg, P.H., and Osten, P. (2004). Sindbis vector SINrep(nsP2S726): a tool for rapid heterologous expression with attenuated cytotoxicity in neurons. Journal of neuroscience methods *133*, 81-90.

Lee, H.K., Min, S.S., Gallagher, M., and Kirkwood, A. (2005). NMDA receptor-independent long-term depression correlates with successful aging in rats. Nat Neurosci *8*, 1657-1659.

Lee, K.H., Lee, J.S., Lee, D., Seog, D.H., Lytton, J., Ho, W.K., and Lee, S.H. (2012). KIF21A-mediated axonal transport and selective endocytosis underlie the polarized targeting of NCKX2. J Neurosci *32*, 4102-4117.

Lee, S.H., Rosenmund, C., Schwaller, B., and Neher, E. (2000). Differences in Ca^{2+} buffering properties between excitatory and inhibitory hippocampal neurons from the rat. The Journal of physiology *525 Pt 2*, 405-418.

Leitch, B., Szostek, A., Lin, R., and Shevtsova, O. (2009). Subcellular distribution of L-type calcium channel subtypes in rat hippocampal neurons. Neuroscience *164*, 641-657.

Luscher, C., and Huber, K.M. (2010). Group 1 mGluR-dependent synaptic long-term depression: mechanisms and implications for circuitry and disease. Neuron *65*, 445-459.

Maccaferri, G., Mangoni, M., Lazzari, A., and DiFrancesco, D. (1993). Properties of the hyperpolarization-activated current in rat hippocampal CA1 pyramidal cells. Journal of neurophysiology *69*, 2129-2136.

Maejima, T., Oka, S., Hashimotodani, Y., Ohno-Shosaku, T., Aiba, A., Wu, D., Waku, K., Sugiura, T., and Kano, M. (2005). Synaptically driven endocannabinoid release requires Ca^{2+}-assisted metabotropic glutamate receptor subtype 1 to phospholipase Cbeta4 signaling cascade in the

cerebellum. J Neurosci *25*, 6826-6835.

Magee, J.C. (1999). Dendritic I_h normalizes temporal summation in hippocampal CA1 neurons. Nature neuroscience *2*, 508-514.

Mannaioni, G., Marino, M.J., Valenti, O., Traynelis, S.F., and Conn, P.J. (2001). Metabotropic glutamate receptors 1 and 5 differentially regulate CA1 pyramidal cell function. J Neurosci *21*, 5925-5934.

Masgrau, R., Servitja, J.M., Sarri, E., Young, K.W., Nahorski, S.R., and Picatoste, F. (2000). Intracellular Ca^{2+} stores regulate muscarinic receptor stimulation of phospholipase C in cerebellar granule cells. Journal of neurochemistry *74*, 818-826.

Masgrau, R., Servitja, J.M., Young, K.W., Pardo, R., Sarri, E., Nahorski, S.R., and Picatoste, F. (2001). Characterization of the metabotropic glutamate receptors mediating phospholipase C activation and calcium release in cerebellar granule cells: calcium-dependence of the phospholipase C response. The European journal of neuroscience *13*, 248-256.

McKay, B.E., McRory, J.E., Molineux, M.L., Hamid, J., Snutch, T.P., Zamponi, G.W., and Turner, R.W. (2006). Ca_V3 T-type calcium channel isoforms differentially distribute to somatic and dendritic compartments in rat central neurons. The European journal of neuroscience *24*, 2581-2594.

Mockett, B.G., Guevremont, D., Wutte, M., Hulme, S.R., Williams, J.M., and Abraham, W.C. (2011). Calcium/calmodulin-dependent protein kinase II mediates group I metabotropic glutamate receptor-dependent protein synthesis and long-term depression in rat hippocampus. J Neurosci *31*, 7380-7391.

Nakamura, T., Barbara, J.G., Nakamura, K., and Ross, W.N. (1999). Synergistic release of Ca^{2+} from IP_3-sensitive stores evoked by synaptic activation of mGluRs paired with backpropagating action potentials. Neuron *24*, 727-737.

Nakamura, T., Nakamura, K., Lasser-Ross, N., Barbara, J.G., Sandler, V.M., and Ross, W.N. (2000). Inositol 1,4,5-trisphosphate (IP_3)-mediated Ca^{2+} release evoked by metabotropic agonists and backpropagating action potentials in hippocampal CA1 pyramidal neurons. J Neurosci *20*, 8365-8376.

Neher, E. (1998). Vesicle pools and Ca^{2+} microdomains: new tools for understanding their roles in neurotransmitter release. Neuron *20*, 389-399.

Oliet, S.H., Malenka, R.C., and Nicoll, R.A. (1997). Two distinct forms of long-term depression coexist in CA1 hippocampal pyramidal cells. Neuron *18*, 969-982.

Otani, S., and Connor, J.A. (1998). Requirement of rapid Ca^{2+} entry and synaptic activation of metabotropic glutamate receptors for the induction of long-term depression in adult rat hippocampus. J Physiol *511 (Pt 3)*, 761-770.

Ransom, C.B., Tao, W., Wu, Y., Spain, W.J., and Richerson, G.B. (2013). Rapid regulation of tonic GABA currents in cultured rat hippocampal neurons. Journal of neurophysiology *109*, 803-812.

Razik, D.S., Hawellek, D.J., Antkowiak, B., and Hentschke, H. (2013). Impairment of GABA transporter GAT-1 terminates cortical recurrent network activity via enhanced phasic inhibition. Front Neural Circuits *7*, 141.

Rebecchi, M.J., and Pentyala, S.N. (2000). Structure, function, and control of phosphoinositide-specific phospholipase C. Physiological reviews *80*, 1291-1335.

Reyes-Harde, M., and Stanton, P.K. (1998). Postsynaptic phospholipase C activity is required for the induction of homosynaptic long-term depression in rat hippocampus. Neuroscience letters *252*, 155-158.

Rubinson, D.A., Dillon, C.P., Kwiatkowski, A.V., Sievers, C., Yang, L., Kopinja, J., Rooney, D.L., Zhang, M., Ihrig, M.M., McManus, M.T., et al. (2003). A lentivirus-based system to functionally silence genes in primary

mammalian cells, stem cells and transgenic mice by RNA interference. Nature genetics *33*, 401-406.

Ryan, X.P., Alldritt, J., Svenningsson, P., Allen, P.B., Wu, G.Y., Nairn, A.C., and Greengard, P. (2005). The Rho-specific GEF Lfc interacts with neurabin and spinophilin to regulate dendritic spine morphology. Neuron *47*, 85-100.

Ryu, S.H., Suh, P.G., Cho, K.S., Lee, K.Y., and Rhee, S.G. (1987). Bovine brain cytosol contains three immunologically distinct forms of inositolphospholipid-specific phospholipase C. Proceedings of the National Academy of Sciences of the United States of America *84*, 6649-6653.

Schnabel, R., Kilpatrick, I.C., and Collingridge, G.L. (1999). An investigation into signal transduction mechanisms involved in DHPG-induced LTD in the CA1 region of the hippocampus. Neuropharmacology *38*, 1585-1596.

Sohn, J.W., Lee, D., Cho, H., Lim, W., Shin, H.S., Lee, S.H., and Ho, W.K. (2007). Receptor-specific inhibition of GABAB-activated K^+ currents by muscarinic and metabotropic glutamate receptors in immature rat hippocampus. The Journal of physiology *580*, 411-422.

Sohn, J.W., Yu, W.J., Lee, D., Shin, H.S., Lee, S.H., and Ho, W.K. (2011). Cyclic ADP ribose-dependent Ca^{2+} release by group I metabotropic

glutamate receptors in acutely dissociated rat hippocampal neurons. PloS one *6*, e26625.

Stell, B.M., and Mody, I. (2002). Receptors with different affinities mediate phasic and tonic $GABA_A$ conductances in hippocampal neurons. J Neurosci *22*, RC223.

Varnai, P., and Balla, T. (1998). Visualization of phosphoinositides that bind pleckstrin homology domains: calcium- and agonist-induced dynamic changes and relationship to myo-[^{3}H]inositol-labeled phosphoinositide pools. The Journal of cell biology *143*, 501-510.

Wang, H.Y., Kuo, Z.C., Fu, Y.S., Chen, R.F., Min, M.Y., and Yang, H.W. (2015). $GABA_B$ receptor-mediated tonic inhibition regulates the spontaneous firing of locus coeruleus neurons in developing rats and in citalopram-treated rats. The Journal of physiology *593*, 161-180.

Won, H., Lee, H.R., Gee, H.Y., Mah, W., Kim, J.I., Lee, J., Ha, S., Chung, C., Jung, E.S., Cho, Y.S., et al. (2012). Autistic-like social behaviour in Shank2-mutant mice improved by restoring NMDA receptor function. Nature *486*, 261-265.

Xu, J.Y., Chen, R., Zhang, J., and Chen, C. (2010). Endocannabinoids differentially modulate synaptic plasticity in rat hippocampal CA1 pyramidal

neurons. PloS one *5*, e10306.

Younts, T.J., Chevaleyre, V., and Castillo, P.E. (2013). CA1 pyramidal cell theta-burst firing triggers endocannabinoid-mediated long-term depression at both somatic and dendritic inhibitory synapses. J Neurosci *33*, 13743-13757.

Younts, T.J., Monday, H.R., Dudok, B., Klein, M.E., Jordan, B.A., Katona, I., and Castillo, P.E. (2016). Presynaptic Protein Synthesis Is Required for Long-Term Plasticity of GABA Release. Neuron *92*, 479-492.

Yuan, B., Latek, R., Hossbach, M., Tuschl, T., and Lewitter, F. (2004). siRNA Selection Server: an automated siRNA oligonucleotide prediction server. Nucleic acids research *32*, W130-134.

ABSTRACT in KOREAN

글루탐산은 뇌에서 작용하는 대표적인 신경전달물질로써 이것은 이온성 글루탐산 수용기(iGluRs)와 대사성 글루탐산 수용체 (mGluRs)를 활성화 시킨다. 이 두가지 타입의 글루탐산 수용체는 서로 상호 작용을하는데 mGluR에 의해서 iGluR이 조절되는 기전은 잘 알려진 반면, iGluR에 의해서 mGluR이 조절되는 기전에 대해서는 알려진 바가 적다. 본 연구에서는 쥐의 해마에서 그룹 1 mGluR 특이적 작용물질인 (RS)-3,5-dihydroxyphenylglycine (DHPG) 단독으로는 phospholipase(PLC)를 활성화 하기 어렵지만, iGluR과 mGluR을 동시에 활성화 시키는 글루탐산에 의해서는 PLC를 강하게 활성화 시키는 것을 관찰하였다. 이러한 결과는 iGluR이 1군 mGluR에 의한 PLC의 활성화에 연관이 되어있음을 시사한다. 본 연구자는 글루탐산에 의해서 활성화된 AMPA 수용체를 시작으로 L-type 칼슘 채널을 통한 칼슘 유입이 mGluR에 의한 PLC 활성화에 특이적으로 필요함을 밝혔다. 더불어 이 매카니즘은 해마에서 저빈도 쌍 자극(paired-pulse low frequency synaptic stimulation(PP-LFS))으로 유도되는 mGluR에 의한 장기억제에

중요함을 확인하였다. 한편, PP-LFS는 시냅스의 억제를 유도하였지만 역설적이게도 입출력 관계에서는 증가를 야기하였다. 이것은 PP-LFS가 mGluR에 의한 엔도카나비노이드(eCB) 시그널링 경로를 통해 억제성 시냅스에서도 장기억제(i-LTD)를 유도하였기 때문이다. 이로 인해 지연성 GABA 전류(tonic GABA current)가 감소됨으로써 활동전압의 역치가 낮아졌고, 이것은 EPSP 와 스파이크 간의 관계에 상승 작용을 가져옴으로서 활동전압의 출력이 증가하였다. 반면, DHPG는 흥분성 시냅스에서는 장기억제를 유도하였지만 억제성 시냅스에서는 장기억제가 거의 일어나지 않았다. 이러한 결과들을 통해 PP-LFS 특이적으로 mGluR에 의한 eCB 시그널링 경로를 통한 억제성 뉴런의 탈억제가 입출력 관계에 중요한 역할을 함을 알 수 있다.

키워드: CA1 피라미드 뉴런, mGluR5, PLC, 칼슘, 전기생리학, mGluR-LTD, 엔도카나비노이드, 지연성 억제, 입출력 관계

Student Number: 2011-23798